Accepted Manuscript

High-fat Diet Accelerates Carcinogenesis in a Mouse Model of Barrett's Esophagus via IL8 and Alterations to the Gut Microbiome

Natasha Stephens Münch, Hsin-Yu Fang, Jonas Ingermann, H. Carlo Maurer, Akanksha Anand, Victoria Kellner, Vincenz Sahm, Maria Wiethaler, Theresa Baumeister, Frederik Wein, Henrik Einwächter, Florian Bolze, Martin Klingenspor, Dirk Haller, Maria Kavanagh, Joanne Lysaght, Richard Friedman, Andrew J. Dannenberg, Michael Pollak, Peter R. Holt, Sureshkumar Muthupalani, James G. Fox, Mark T. Whary, Yoomi Lee, Tony Y. Ren, Rachael Elliot, Rebecca Fitzgerald, Katja Steiger, Roland M. Schmid, Timothy C. Wang, Michael Quante

High-fat Diet Accelerates Carcinogenesis in a Mouse Model of Barrett's Esophagus via IL8 and Alterations to the Gut Microbiome

Short title: HFD accelerates esophageal carcinogenesis

Natasha Stephens Münch[1 2#], *Hsin-Yu Fang*[1#], *Jonas Ingermann*[1 2#], *H. Carlo Maurer*[1 3], *Akanksha Anand*[1], Victoria *Kellner*[1], *Vincenz Sahm*[1], *Maria Wiethaler*[1], *Theresa Baumeister*[1], *Frederik Wein*[1], *Henrik Einwächter*[1], *Florian Bolze*[2 4 5], *Martin Klingenspor*[2 4 5], *Dirk Haller*[6], *Maria Kavanagh*[7], *Joanne Lysaght*[7], *Richard Friedman*[3], *Andrew J. Dannenberg*[8], *Michael Pollak*[9], *Peter R Holt*[10], *Sureshkumar Muthupalani*[11], *James G. Fox*[11], *Mark T. Whary*[11], *Yoomi Lee*[3], *Tony Y. Ren*[3], *Rachael Elliot*[12], *Rebecca Fitzgerald*[13], *Katja Steiger*[14], *Roland M. Schmid*[1], *Timothy C. Wang*[3], *Michael Quante*[1]*

[1]Department of Internal Medicine, Technical University of Munich, Germany
[2]Chair of Molecular Nutritional Medicine, Technical University of Munich, Germany[3]Irvine Cancer Research Center, Columbia University, New York, USA
[4]EKFZ – Else Kröner-Fresenius Center for Nutritional Medicine, Technical University of Munich, Germany
[5]ZIEL – Institute of Food & Health, Technical University of Munich, Germany
[6]Chair of Nutrition and Immunology; Technical University of Munich, Germany
[7]Department of Surgery, Trinity Translational Medicine Institute, Trinity College Dublin, Ireland
[8]Weill Cornell Medical College, New York, NY, USA
[9]McGill University, Montreal, Quebec, Canada
[10]Rockefeller University, New York, NY, USA
[11]Massachusetts Institute of Technology, Cambridge, MA, USA
[12]University of California San Francisco, CA, USA
[13]Cambridge University, Cambridge, UK
[14]Institute of Pathology, Technical University of Munich, Germany

*Correspondence: michael.quante@tum.de (M.Q.)
[#]authors contributed equally

Conflicts of interests: none

Author contributions:

NSM, HYF, JI performed experiments, analyzed data and wrote the manuscript,
MK, MK, JL, YL, FW, HCM, VK, VS, MW, TB, SIS, AA, FB, JL, MTW, MK and DH performed experiments and analyzed data
RF, HE performed bioinformatics
PRH, AJD performed human serum study, analyzed data and edited manuscript
MP quantified analytes in human serum
SM, JGF performed germfree experiments and analyzed data
RE, RF performed human microbiome experiments and analyzed data
KS performed histopathological evaluation
RMS analyzed data and provided funding
TCW analyzed data, wrote the manuscript, provided funding
MQ designed and supervised the study, analyzed data, wrote the manuscript, provided funding

Abbreviations:
BE (Barrett's esophagus), EAC (Esophageal adenocarcinoma), GEJ (Gastroesophageal junction) GERD (Gastro-esophageal reflux disease), GF (germfree) HFD (High fat diet), NK cells(Natural killer cells),SCJ (squamocolumnar junction), WT (Wildtype)

Funding:

The research leading to these results has received funding from the Deutsche Forschungsgemeinschaft (DFG) under Grant Agreement No. SFB 824 and has been funded by the Deutsche Krebshilfe with in the Max Eder Program to MQ. Additionally, TCW (PI) and MQ were funded by the NCI Barrett's Esophageal Translational Research Network (2 U54 CA163004-06). JI, NSM, MQ, DH MK were funded by a graduate program by the German Research Fund (GRK 1482)

Gene Expression Analysis:
Raw data have been deposited in National Center for Biotechnology Information's Gene Expression Omnibus (GEO) (GSE103616)

Abstract

Background & Aims: Barrett's esophagus (BE) is a precursor to esophageal adenocarcinoma (EAC). Progression from BE to cancer is associated with obesity, possibly due to increased abdominal pressure and gastroesophageal reflux disease, although this pathogenic mechanism has not been proven. We investigated whether environmental or dietary factors associated with obesity contribute to progression of BE to EAC in mice.

Methods: Tg(ED-L2-IL1RN/IL1B)#Tcw mice (a model of BE, called L2-IL1B mice) were fed a chow (control) or high-fat diet (HFD), or crossbred with mice that express human IL8 (L2-IL1B/IL8 mice). Esophageal tissues were collected and analyzed for gene expression profiles and by quantitative PCR, immunohistochemistry, and flow cytometry. Organoids were established from BE tissue of mice and cultured with serum from lean or obese individuals, or neutrophils from L2-IL1B mice. Feces from mice were analyzed by 16s rRNA sequencing and compared to 16s sequencing data from patients with dysplasia or BE. L2-IL1B were mice raised in germ-free conditions.

Results: L2-IL1B mice fed a HFD developed esophageal dysplasia and tumors more rapidly than mice fed the control diet; the speed of tumor development was independent of body weight. The acceleration of dysplasia by the HFD in the L2-IL1B mice was associated with a shift in the gut microbiota and an increased ratio of neutrophils to natural killer cells in esophageal tissues, compared to mice fed a control diet. We observed similar differences in the microbiomes from patients with BE that progressed to EAC vs patients with BE that did not develop cancer. Tissues from dysplasias of L2-IL1B mice fed the HFD contained increased levels of cytokines that are produced in response to CXCL1 (the functional mouse homolog of IL8, also called KC). Serum from obese patients caused organoids from L2-IL1B/IL8 mice to produce IL8. BE tissues from L2-IL1B mice fed the HFD and from L2-IL1B/IL8 mice contained increased numbers of myeloid cells and cells expressing *Cxcr2* and *Lgr5* mRNAs (epithelial progenitors) compared to mice fed control diets. BE tissues from L2-IL1B mice raised in germ-free housing had fewer progenitor cells and developed less dysplasia than in L2-IL1 mice raised under standard conditions; exposure of fecal microbiota from L2-IL1B mice on HFD to L2-IL1B mice on control diet accelerated tumor development.

Conclusions: In a mouse model of BE, we found that a HFD promoted dysplasia by altering the esophageal microenvironment and gut microbiome, thereby inducing inflammation and stem cell expansion, independent of obesity.

Keywords:

NK cells, neutrophils, cytokines, IL1B

Introduction

BE is thought to arise as a consequence of gastro-esophageal reflux disease (GERD), which damages the esophageal mucosa, leading to a replacement of squamous epithelium by a metaplastic columnar epithelium above the gastroesophageal junction (GEJ)[1]. The increase in EAC incidence in the Western world has led to some uncertainty in the clinical management of BE and the estimation of its risk for EAC. While current strategies employ aggressive screening, surveillance and/or ablation procedures, the benefits of such procedures have been difficult to demonstrate[2] and a better understanding of risk factors is needed.

In addition to male gender, age and tobacco use[3], obesity is strongly associated with the development of EAC[4] and is now endemic in Western countries and Asia. Obesity or a high waist circumference are thought to promote BE/EAC through increased abdominal pressure and GERD[5], although this mechanism has not been proven and the degree of GERD correlates poorly with disease progression. Evidence linking obesity to cancer risk derives primarily from observational cohort studies, which may not establish directly causality, but identified associations of multiple obesity-related factors (hormones, cytokines, adipokines) with increased risk and poor outcome. In this context, obesity is mostly used as a proxy for an underlying but still undefined mechanism[6]. This leaves the possibility that environmental or dietary factors that are prevalent in obese patients influence the risk of BE progression, rather than increased body fat per se[7], as recently demonstrated for colorectal cancer[8]. Changes in diet can lead to alterations in the gut microbiome[9], with effects on stem cell biology[10] and thus the susceptibility to gastrointestinal neoplasia. Furthermore, a Western-style diet itself can contribute to chronic inflammation[8, 11, 12], which itself can favor the emergence of gut microbiota that favor carcinogenesis[13].

Here, we utilize the L2-IL1B mouse model of BE[14] to analyze dietary effects of a HFD on BE progression. The L2-IL1B mouse model expresses human interleukin 1β in the esophagus and forestomach squamous epithelium, resulting in inflammation with progression to metaplasia and dysplasia. We demonstrate that HFD leads to global changes in the gut microbiome that mirror closely those observed in BE patients, and facilitates the establishment of an inflammatory pro-carcinogenic microenvironment at the GEJ accelerating disease progression.

Important Methods

Animals

The mouse model (L2-IL1B, Tg(ED-L2-IL1RN/IL1B)#tcw)[14], was backcrossed to C57BL/6J mice and fed a standard Chow diet from birth until weaning, and water *ad libitum*. Between 6 and 8 weeks of age, mice were started on HFD, control diet or remained on the Chow (ssniff). For bedding transfer experiments, cages were filled half with fresh bedding, while the other half was bedding from HFD cages starting at the age of 6 weeks until 9 months. IL8 mice[15] and Mc4rX16 mice[16] were bred with L2-IL1B, mice to obtain L2-IL1B/IL8Tg mice and L2-IL1B/Mc4R mice. Germfree mice were generated by embryo transfer rederivation of conventional L2-IL1B mice into germfree Swiss recipient mothers[17] and maintained in sterile isolators on autoclaved food (RMH3000, Purina, USA) comparable to the standard chow and water (Suppl. Figure 8). Sterility was confirmed every other week by 16s PCR, aerobic, anaerobic and fungal culture as well as Gram stains of fecal smears. Animal experiments were approved by the District Government of Bavaria and performed in accordance with the German Animal Welfare and Ethical Guidelines and by the Committee on Animal Care at the MIT, USA.

Tissue preparation and disease evaluation

Macroscopic scoring of the squamocolumnar junction (SCJ) and the esophagus was performed and scores averaged as shown in Suppl. Fig. 1B, C. For further RNA or protein analysis the SCJ was macroscopically identified as the first 2 mm of columnar tissue and cut with a magnifying glass dissection-scope to eliminate squamous tissue contamination as good as possible. Mouse tissues were fixed in formalin and paraffin-embedded then cut and stained with H&E (Haematoxylins and eosin). *Histopathological scores were performed by an experienced mouse pathologist b*y previously established criteria for the influx of immune cells per high-power field, metaplasia and dysplasia[14] (Suppl. Fig 1D): *Inflammation was scored by the percentage of different immune cells (mostly neutrophilic myeloid cells) in a defined tissue area of the SCJ in a high-power field evaluation. Metaplasia was evaluated by the abundance of mucus producing or cells per gland and the abundance of glands with mucus producing cells in the BE area at the SCJ. Dysplasia was evaluated by the amount of cellular atypia and the presence of low or high grade dysplasia in single or multiple glands as assessed by experienced mouse pathologists.* Mucus production was assessed by Periodic

Acid-Schiff- (PAS) staining and quantified as percentage of PAS positive area in BE regions. Crypt fission was quantified by counting fused crypts in the BE region.

Statistics

Statistical analysis was performed using Graph Prism 6 with Student's t-tests or one-way or two-way ANOVA's with p-values noted in each corresponding figure. For 2-way ANOVA, Sidak-Holm post-hoc was used, for 1 way ANOVA, Tukey post-hoc was used.

Results

HFD accelerates esophageal dysplasia in the L2-IL1B mouse model, independent of obesity

To study the effect of diet on BE and EAC, we fed wild type (WT) and L2-IL1B mice either Chow or high fat diet (HFD, 48% fat, Suppl. Fig. 1A). No pathological phenotype at the squamocolumnar junction (SCJ) in Chow and HFD fed WT mice (Fig. 1A-F, Suppl. Fig. 1B, C, D), in contrast to L2-IL1B mice on both diets. Compared to Chow fed L2-IL1B mice, a significant increase in macroscopic tumor burden at the SCJ and in the esophagus was observed in L2-IL1B mice on HFD at 9 and 12 months (Fig. 1A, B). Both L2-IL1B mice on HFD and Chow diet developed increasing but similar amounts of inflammation and columnar metaplasia over time (Fig. 1A, C, D, F). However, HFD-treated L2-IL1B mice exhibited a significant increase in proliferation only at the age of 12 months (Fig. 1A,G) compared to chow fed L2-IL1B mice. This correlated with markedly elevated dysplasia scores in HFD fed L2-IL1B mice as early as 9 months (Fig. 1A, E), demonstrating an accelerating effect of HFD on esophageal carcinogenesis in the mouse model.

In contrast to HFD-induced obesity in WT mice (48% weight gain ($p<0.001$)), HFD-fed L2-IL1B mice did not gain body weight ($p<0.001$) (Fig. 1H). Both fat and lean mass were lower in L2-IL1B mice on HFD relative to WT mice on HFD (Suppl. Fig. 1E). Thus, acceleration of the BE phenotype occurred independent of body weight (Fig. 1I). To examine whether obesity alone without an additional inflammatory component was sufficient to influence BE progression, we interbred the L2-IL1B mice with mice lacking a functional melanocortin-receptor-4 ($Mc4r^{W16X}$)[16], which exhibit an obese phenotype comparable to HFD-induced obesity and are modeling the most common monogenic cause for obesity in humans[18] (Suppl. Fig. 2A-C). L2-IL1B mice with a heterozygous ($Mc4r^{+/-}$ or $Mc4r^{het}$) or homozygous ($Mc4r^{-/-}$ or $Mc4r^{ki}$) loss of Mc4r showed a similar BE phenotype as L2-IL1B mice on a chow diet. In contrast to L2-IL1B mice on a HFD, $Mc4r^{het;}$ L2-IL1B mice showed an absence of disease acceleration, with no increase in the level of inflammation, metaplasia or dysplasia (Suppl. Fig. 2A,D-G). There was no increase in the expression of inflammatory cytokine (data not shown), splenomegaly (Suppl. Fig. 2H) in L2-IL1B/$Mc4r^{het}$ and L2-IL1B/$Mc4r^{ki}$ mice, compared to L2-IL1B mice (Suppl. Fig. 2I)[14]. These data suggest that genetic obesity does not promote BE progression, and HFD accelerates the phenotype independent of body weight.

HFD induces an immune response leading to a distinct local inflammatory reaction

Previously, we showed that overexpression of IL1B in the esophagus leads to upregulation of pro-inflammatory cytokines[14]. HFD promotes chronic inflammatory responses, as has been demonstrated for colorectal carcinogenesis[8]. Thus, we postulated that the enhancement of dysplasia in L2-IL1B mice by HFD might be due primarily to a change of systemic and esophageal inflammation profiles. Although our tissue inflammation metric was not significantly altered in HFD L2 mice compared with chow fed L2 mice (Fig. 1C), Gene-expression (Fig. 2A) and Gene-Set-Enrichment-Analysis (GSEA) (Suppl. Fig. 3A) of SCJ tissue revealed changes in cytokine expression associated with HFD. Key mediators of this cytokine response were related to cell survival, proliferation, angiogenesis, apoptosis and importantly chemoattraction for the observed immune cells (Fig. 2A, B and Suppl. Fig. 3B). $aSMA^+$ myofibroblasts within the SJC region were significantly increased in HFD fed L2-IL1B mice (Fig. 2E), indicating an activated stromal reaction associated with the inflammatory response.

Serum from L2-IL1B mice fed with HFD significantly stimulated the growth of 3D mouse BE organoids (Fig. 2C), compared to serum from Chow mice, suggesting that systemic inflammatory components affect epithelial cell growth. Of note, serum analysis of 20 obese versus non-obese patients revealed that the pro-inflammatory cytokines IL-6 and leptin were elevated, and adiponectin decreased (Suppl. Fig. 4A). Additionally, we observed an upregulation of chemokines involved in recruitment and/or differentiation of myeloid cells and T cells, such as CCL6, CCL12 and G-CSF, (Fig. 2B, Suppl. Fig. 3B) in esophageal tissue in L2-IL1B mice on HFD. Importantly, the functional mouse homolog of IL8, KC or CXCL1, was among those cytokines in the chemokine array (Fig 2B), and was also upregulated 6-fold in esophagus tissue lysates from L2-IL1B mice on HFD for 12 months (Fig. 2D). Thus, HFD activates a systemic immune response that also affects the local microenvironment. Cytokine arrays of SCJ and esophageal tissue in Chow and HFD fed WT mice did not show any major changes; nevertheless, serum from WT-HFD showed a mainly obesity related phenotype, compared to chow fed WT mice, whereas HFD fed L2-IL1B mice showed an accelerated inflammatory phenotype compared to Chow fed L2-IL1B mice (Suppl. Fig.3C).

HFD leads to levels of IL8/KC chemokines that promote esophageal dysplasia

Esophageal tissue IL8 expression has been shown to be associated with histopathological inflammation in 50 BE patients and has been hypothesized to play a role in esophageal carcinogenesis[19]. Consistent with these earlier clinical observations, levels of the functional mouse IL8 homologue, KC or CXCL1[20], were significantly increased in the esophagus of HFD fed L2-IL1B mice (Fig. 2B, D). We also noted increased IL8 levels in conditioned media of a human EAC compared to BE or squamous cell lines (Fig. 2 F), and increased IL8 levels in conditioned media from BE and EAC esophageal biopsies compared to normal and esophagitis (Fig. 2G). Since rodents lack the IL8 gene, we crossed a human IL8-BAC-transgenic mouse model[15], which exhibits tissue specific, physiologic IL8 gene regulation, with the L2-IL1B mice to generate L2-IL1B/IL8Tg mice. L2-IL1B/IL8Tg mice showed an accelerated phenotype, remarkably similar to that of L2-IL1B HFD mice (Fig. 3A-C, Suppl. Fig 4B), with a 2-fold increase in dysplasia scores (Fig. 3D), along with increased proliferation (Fig. 3E) and differentiation (Fig. 3F). Furthermore, we observed significant increases in $aSMA^{+}$ stromal myofibroblasts (Fig. 3G).

Utilizing gene expression data from L2-IL1B/IL8Tg compared to L2-IL1B mice, we generated an IL8 specific gene set including 150 upregulated and 110 downregulated genes. Genes stimulated by IL8 pathway activity were enriched in HFD fed WT and L2-IL1B mice compared to Chow fed mice (Fig. 3H), suggesting that the IL8/CXCL1 chemokine family contributes to the observed HFD L2-IL1B phenotype. However, we could not detect a difference in serum IL8 levels (Suppl.Fig. 4C) nor a correlation with obesity (Suppl. Fig. 4D) in patients with BE, LGD, HGD or EAC. Instead, elevated tissue concentrations of IL8 measured in conditioned medium from human patient biopsies (Fig. 2G), suggested that IL8 acts at a local level. When we treated BE organoids from L2-IL1B/IL8Tg mice with lean or obese human sera, obese sera stimulated growth of BE organoids (Suppl. Fig.4E). Relative to lean serum treatment, obese serum resulted in higher levels of L2-IL1B/IL8Tg mouse epithelial cell derived IL8 in the supernatant (Fig. 3I), indicating that serum components from obese subjects could induce local epithelial IL8 secretion. These data demonstrate that IL8 secretion in esophageal tissue is induced by HFD and plays an important role in stimulating BE cell proliferation *in vitro* and *in vivo*.

HFD increases neutrophils and decreases NK cells at the SCJ

Assessment of the immune cell infiltrate in the lower esophagus using FACS (Suppl.Fig. 5A) in 12-month old L2-IL1B HFD mice with dysplasia showed a significant increase in neutrophils and immature myeloid cells (IMC) (Fig. 4A), previously linked to the IL8 pathway[15]. No differences in macrophages, CD4 helper T-cells, CD8 cytotoxic T-cells or gamma-delta T-cells were observed (Suppl. Fig. 5B). The influx of granulocytic myeloid cells was confirmed by IHC of the SCJ and lower esophagus (Fig. 4B) and was not observed in the glandular stomach (data not shown), highlighting the specificity of the response for the SCJ. Additionally, we observed a significant decrease in NK cells in HFD compared to chow fed mice (Fig. 4A), suggesting an inhibitory effect by neutrophils on NK cells, as previously reported[21]. We also found increased neutrophils in esophageal tissue of L2-IL1B/IL8Tg mice (Fig. 4C, D), consistent with the known role of IL8 as a recruiter of granulocytic immune cells[15], while no difference could be detected for other immune cells (Suppl. Fig. 6A, B). Importantly, a significant increase of immune cells expressing IL8 receptor CXCR2 was observed in L2-IL1B HFD and L2-IL1B/IL8-Tg mice compared to L2-IL1B mice (Fig. 4E,F).

Co-cultured mouse BE organoids with neutrophils from the spleens of 9-12 months old L2-IL1B mice demonstrated a significant increase in proliferation and organoid growth in a dose-dependent fashion suggesting a direct stimulatory effect of neutrophils on BE epithelial cells (Fig. 4G). This response was mediated by inflammatory cytokines, such as leptin and IL-10, which were secreted solely under organoid-neutrophil co-culture conditions (Fig 4H,I).

The esophageal inflammatory niche recruits SCJ progenitor cells

In addition to elevated CXCR2+ immune cells, we observed increased CXCR2 expressing epithelial cells in BE regions during disease progression (Fig. 5A), suggesting an effect of the inflammatory microenvironment on a distinct epithelial cell population. Previous studies by our group[14] and others[22] have pointed to the gastric SCJ[23] as the origin of BE and EAC, with expansion of SCJ progenitor cells into the esophagus in response to chronic inflammation, thus giving rise to metaplastic and dysplastic lesions[1]. Indeed, when we analyzed gene expression changes related to HFD and IL8 expression, we observed a highly significant enrichment of stem cell signatures (Fig. 5B,C). In situ hybridization revealed a significant increase of the naturally present Lgr5^{+} progenitor cells[24] in areas of BE at the SCJ in L2-IL1B mice on HFD, compared to Chow, and in L2-IL1B/IL8Tg mice (Fig. 5D). Lgr5+ cells could be found in the typical location at the bottom of the first SCJ crypt as well as in the BE region at the SCJ. These findings suggest that IL8/KC family members may directly stimulate through CXCR2

the expansion of Lgr5 progenitor cells at the SCJ. Indeed, Lgr5+ cells in HFD fed L2-IL1B mice highly expressed the IL8 receptor, CXCR2, and Lgr5+ cells increased with dysplastic progression (Fig. 5E). Additionally, analysis of BE specimens from 12-month old L2-IL1B HFD and L2-IL1B/IL8Tg mice showed significantly more crypt fission compared to age-matched L2-IL1B chow fed mice (Fig. 5F). These observations suggest a mechanism by which activation of SCJ progenitor cells by HFD/IL8 through CXCR2 could lead to crypt fission and expansion of SCJ glands into the esophagus, thus giving rise to metaplasia and dysplasia.

HFD altered intestinal microbiota promote the accelerated immune response and dysplasia phenotype

Diet affects the composition of gut microbiota[9] and dysbiosis is linked to cancer development[13]. Previously, a modest reduction in microbial diversity in BE tissue in the human esophagus was shown[25], matching our results from 16S-rRNA gene sequencing of bacterial DNA isolated from the mouse SCJ. No clustering could be observed in the tissue from WT or L2-IL1B mice (Suppl. Fig. 7A) suggesting that esophageal microbes are difficult to categorize in their role during carcinogenesis.

Since the lower GI tract harbors the majority of the intestinal microbiota, which mediate much of the dietary effects, we analyzed the intestinal microbiota by 16S-rRNA gene sequencing of fecal samples from 6-month-old WT and L2-IL1B mice on Chow, HFD, or nutrient-matched experimental diet[26] (referred to as 'Control', Suppl. Fig. 8A). There was no difference in the SJC histopathology between Control and Chow, indicating that HFD, rather than the purified nutrient component, was responsible for the accelerated phenotype (Fig.6F, Suppl.Fig. 8B-E). Analysis of microbial β-diversity showed separate clustering of HFD fed L2-IL1B mice compared to all other groups, with a unique taxonomic profile, while WT and L2-IL1B harbored very microbiota on control and on chow (Fig. 6A). Importantly, we observed an altered *Firmicutes* to *Bacteroidetes* ratio in HFD fed mice (Fig. 6B, Suppl. Fig. 7B,C), which correlated well with the increased *Firmicutes: Bacteroidetes* ratio in previously published patient (BE and HGD) data[25] (Fig. 6B), although these data were from different tissue sites (feces versus esophagus) and comparisons of the microbiota between two species must be made cautiously.

To investigate whether the gut microbiota in general influenced inflammation and tumor development in the L2-IL1B HFD mouse model, we re-derived L2-IL1B mice as germfree (GF) and found a marked

reduction of inflammation, metaplasia and dysplasia, with an increase in goblet-like cells (Fig. 6C, D, Suppl.Fig 6C). This correlated with a significantly reduced influx of neutrophils and IMCs into the esophagus of germfree L2-IL1B mice (Fig. 6E), directly linking the elimination of enteric microbes to the inflammatory phenotype. Lgr5+ and Cxcr2+ cells at the SJC were significantly decreased under germfree conditions (Fig. 5A,D). When transferring bedding including feces from L2-IL1B mice on HFD to cages of L2-IL1B mice on Control diet over 9 months, the tumor phenotype could be transmitted, suggesting that the fecal microbial community is at least partly responsible for the SCJ phenotype (Fig. 6F and Suppl.Fig. 8F). Changes in the microbial community structure from HFD fed L2-IL1B mice pointed to unique functions, as the well-established PICRUSt pipeline[27] *in silico* analysis of 16S-rRNA genes generated a predictive metagenome in KEGG pathway analysis. Clustering KEGG data showed that in L2-IL1B mice, HFD differentiated microbial function from Chow and Control diet (Fig. 6G). Functional pathway differences between HFD and Control in L2-IL1B mice[27] (Fig. 6H, Suppl.Fig. 7D) suggest a microbial HFD associated component contributing to disease acceleration. One of the mostly regulated pathways in KEGG analysis in HFD fed L2-IL1B mice was bacterial Lipopolysaccharides (LPS) biosynthesis (Fig. 6I), known to have effects on inflammatory responses. GSEAs revealed an upregulation of the inflammatory response to LPS and Toll-Like Receptor (TLR) signaling in the SCJ of L2-IL1B HFD mice, suggesting that such gut microbiota changes are likely influenced through TLR signaling (Fig. 6J, K and Suppl. Fig 7E).

Discussion

The increase in BE and EAC in developed countries points to pathogenetic environmental influences. However, the increase in obesity[32-35] did not precede this rise in EAC as one might suspect for a causative factor[28]. We provide evidence for an alternative hypothesis, suggesting that obesity and BE/EAC are secondary to the increasing consumption of a western-style or HFD[7]. HFD accelerated BE progression in the L2-IL1B mouse model through effects on gut microbiota, demonstrating the importance of the microbiome, and linking its influence in part to activity of the IL8/CXCL1 chemokine family within a distant altered inflammatory microenvironment.

HFD induced obesity in WT mice but not in L2-IL1B mice, where it accelerated the BE/EAC phenotype. The absence of weight gain in L2-IL1B mice on HFD was likely due to systemic effects of IL1B, but also raises the question as to whether increased body fat alone contributes to BE/EAC. In contrast to the HFD model, a genetic model of obesity ($Mc4r^{x16}$) did not increase BE progression, arguing against body weight alone as a driver of esophageal carcinogenesis in mice. Instead, disease acceleration correlated with increased inflammation[29], through pro-inflammatory cytokines and chemokines[30] altering the local microenvironment with accumulation of immune cells and αSMA+ fibroblasts, which are known to recruit immune cells through specific factors (VEGF, HGF, MMP2, and IL8)[31].

In our initial report of L2-IL1B mice, we noted upregulation of IL-6, a downstream target of IL1B, whose genetic ablation could attenuate the phenotype[14]. Here, we demonstrate a role for HFD in BE progression through inflammatory factors such as the IL8/CXCL1 family of chemokines[14]. The IL8/CXCL1 chemokine family is an additional well-defined downstream target of IL1B, and we observed elevated levels of the functional murine homolog CXCL1 at the SCJ of HFD treated L2-IL1B mice. Other studies have also suggested that chemokines such as IL-8 and IL1B are involved in esophageal carcinogenesis, and that CXCR1 and CXCR2 are expressed in esophageal mucosa[32]. During disease progression, human BE tissue produces abundant IL8, which is strongly overexpressed in EAC patients, pointing to an important role in human carcinogenesis[19]. Together with the observed elevation of CXCL1 gene and protein levels, and most importantly, the finding that immature myeloid cells and neutrophils were mainly attracted to the SCJ, this led us to further examine the effect of IL8 pathway in our mouse model. Indeed, reconstitution of the human IL8 gene in the BE mouse model resulted in acceleration of dysplasia, mimicking the HFD phenotype,

confirming the importance of local IL-8 expression.[33] In this study, we were not able to investigate comprehensively other inflammatory mediators, whether expressed locally or systemically. It has previously been demonstrated that circulating cytokines, including IL8, are associated with increased risk for BE[34] and could be used as potential biomarker[35]. Nevertheless, IL8 likely plays a key local role during esophageal carcinogenesis[19], with the IL8 specific gene signature being enriched in GSEA analysis of HFD fed L2-IL1B mice. IL8 is known to be upregulated by pro-inflammatory cytokines or pathogen-associated factors through toll-like receptors (TLRs)[36], likely through an alteration of the gut microbiome. Although we cannot prove directly in our work that a specific microbial species is activating IL8 signaling in the esophagus, we provide evidence in our KEGG analysis: The bacterial community profile associated with LPS biosynthesis, known to activate TLR signaling, was upregulated in the SCJ of L2-IL1B HFD mice. We would therefore speculate, that gut microbiota changes on the immune system are influenced through TLR signaling, which in turn has an effect on IL8 activation, which is known to activate granulocytic myeloid cells that appear essential to the BE phenotype.

IL8 is a chemoattractant for myeloid cells through its cell surface receptors, CXCR1 and CXCR2[15]. In HFD fed L2-IL1B and L2-IL1B/IL8Tg mice, we observed an accumulation of CXCR2+ IMCs and neutrophils. In combination with organoid culture data, these findings suggest that dietary fat components can result in increased local secretion of IL8/CXCL1 chemokines that then promote the accumulation of immature, granulocytic cells in the esophagus. These observations are consistent with previous studies that reported an increase in IMCs resulting from HFD feeding of WT mice[37], and *H. felis* infection of WT mice[11]. Of note, bile acid treated L2-IL1B mice also exhibit a granulocytic shift, along with acceleration of dysplasia at the SCJ region[14] pointing to the importance of neutrophils.

IMCs can carry out both, tumor promoting and immunosuppressive functions[38]. A subtype comprising CD11b+Ly6G^{high}Ly6C^{low} neutrophils and CD11b+Ly6G^{low}Ly6C^{high} IMCs likely contributes to epithelial growth and progression, as demonstrated in 3D organoid cultures. However, myeloid cells may also possess immunosuppressive properties that could modulate tumor immunity. Tumor-derived *G-CSF* can promote the differentiation of IMCs into immunosuppressive neutrophils[39] that inhibit cytotoxic T-cell responses, thereby facilitating tumor growth and metastasis[40]. Upregulation of G-CSF in HFD fed L2-IL1B mice underlines this possibility of increased myeloid suppressor cell recruitment and/or

differentiation into an immunosuppressive local phenotype. While there was no significant change in cytotoxic T-cell numbers, increases in neutrophils were accompanied by reduced NK cells. Indeed, neutrophils protect against NK cell mediated clearance of tumor cells[21] and have been proposed as a positive prognostic markers in esophageal cancer[41]. Although there are clearly limitations to studies of inflammation in a pro-inflammatory mouse model of BE, the findings suggest that an altered neutrophils to NK ratio may portend a poor prognosis, as shown in other cancers[42].

Apart from IL8 effects on the esophageal inflammatory niche, we observed an epithelial effect of the IL8/CXCL1 chemokine family, with an expansion in the gastric SCJ of Cxcr2 expressing Lgr5+ progenitor cells with accelerated dysplasia. The increase in crypt fission at the SCJ is likely related to this expanded stem/progenitor cell pool. Thus, the transition of the normal SCJ niche to a distinct IL8 driven inflammatory niche may enhance the expansion of BE lesions into the esophagus, a scenario similar to that recently described in skin lesions[43], providing a mechanism for HFD to influence tissue regeneration and cancer incidence[44, 45].

The gut microbiome is modulated by diet[46], and growing evidence indicates that both the microbiome[9] and dietary components[8] can potentiate cancer risk as shown for intestinal cancer[13]. However, such an interaction has not yet been reported for esophageal carcinogenesis. Esophageal carcinogenesis was attenuated under germfree conditions, with reduced influx of immune cells and decreased expansion of stem and epithelial cells. As suggested by previous studies[47,48] and in line with reduced Cxcr2 expressing cells in germfree mice, epithelial IL8 secretion was likely induced by the gut microbiota. We propose that alterations in the esophageal immune niche might be related to body wide inflammatory effects of an altered gut microbiome as reported already for metabolic diseases[49], and as such play a key role in esophageal carcinogenesis. The findings may be relevant to the care and treatment of patients with BE, as dietary modifications could change the gut microbial community and delay or prevent BE progression. Moreover, one could speculate that elimination of specific microbial species through antibiotics might provide a potential tool for cancer prevention. Nevertheless, such commensal bacteria have yet to be identified and further studies are needed to elucidate the role of the gut and/or esophageal microbiome in predicting the development of BE[50]. While GERD and bile acid reflux are known to induce inflammation in the esophagus and believed to contribute to the development of early BE, the gut microbiome may play an important role in malignant progression through acceleration of the inflammatory microenvironment.

While there are alterations in the composition of the microbial community in EAC, there were only modest reductions in microbial diversity in human BE samples[25]. In accordance, we found only modest changes in the microbiota at the SCJ in L2-IL1B mice, while microbial composition in the colon was changed upon feeding HFD, with an altered Firmicutes:Bacteroidetes ratio that correlated with BE progression. This ratio, together with a lower microbial α-diversity, have been associated with HFD[46] and mirrored the changes seen in BE patients. Although the fecal material may not fully reflect the changes in the microbiota colonizing the gastroesophageal region, we would suggest that the fecal microbiota is highly relevant, and may have a systemic impact on BE progression. Changes in gut microbiota may account for the inflammatory phenotype observed in HFD L2-IL1B mice and importantly, can induce an increased cancer phenotype, if transferred to L2-IL1B mice on chow diet. 16S-rRNA gene profiling under diet-controlled conditions demonstrated that the HFD component was responsible for this effect. The esophageal microbiota in humans is thought to be transitory, and may change in association with esophagitis[51], whereas the microbiota of the lower GI tract is quantitatively much greater, with potential systemically mediated inflammatory effects. Indeed, the "pathogenic microbial community" theory suggests that the entire microbial community contributes to pathogenicity, even though no individual community members can be clearly categorized as causative pathogens[52]. We noted a correlation between TLR signaling in GSEA and upregulation of TLR2 in the esophagus, linking the alteration of the gut microbiota to IL8 signaling. In terms of a preventive antibiotic treatment for patients with BE the knowledge of distinct components of the microbiome seems essential, as too long term antibiotic treatment seems to be a difficult option and broad short term antibiotic treatment will result in a fast reconstitution of commensal bacteria [53].

In summary (Suppl. Fig. 9), we propose here that a diet enriched in fat, rather than increased body weight, is responsible for accelerated esophageal carcinogenesis. While IL-1B-dependent chronic inflammation on its own can cause dysplasia, HFD accelerates this disease phenotype by altering the intestinal microbiome and inducing a distinct inflammatory response in the esophagus marked by IL8/KC chemokines. Increased esophageal IL8 expression alters the neutrophils/NK cell ratio and promotes the expansion at the SCJ of Cxcr2+ progenitors that eventually progress to dysplasia. These findings offer some potential new strategies for prevention of BE and EAC and should be investigated further in patient cohorts.

Figure Legends

Figure 1. HFD accelerates esophageal dysplasia in the L2-IL1B mouse model.

(A) (i) macroscopic image and epresentative pictures of (ii) Haematoxylin & Eosin (H&E), (iii) Periodic acid–Schiff (PAS) and (iv) Ki67 of the SCJ. A WT Chow mouse was used as a representative for all WT mice. Macroscopic tumor score at 3-12 months (mean ±SEM) (B), inflammation (C) metaplasia (D), and dysplasia scores (E) (n=8-12, mean ± SD). Quantification of (F) PAS and (G) Ki67 staining (n=8-12). (H) Body weight of L2-IL1B mice. (I) Correlations between body mass and dysplasia score. Quantification of 4 high-magnification-field (20X) of esophagus and SCJ tissue (****p<0.0001, ***p<0.001, **p<0.01, *p<0.05) For (B-E) 2-way ANOVA with Sidak-Holm post-hoc was used, for (F,G) a 1 way ANOVA with Tukey post-hoc and for (H,I) 2 way ANOVA with Tukey Post-hoc. BE region was defined as the region between squamous epithelium and oxyntic mucosa of the stomach. L2=L2-IL-1β, WT=wildtype, HFD=High fat diet

Figure 2. HFD induces a systemic immune response leading to a distinct local inflammatory microenvironment reaction

(A) Gene expression analysis from SCJ tissue (n=3). (B) Cytokine array for chemoattractants of immune cells and cytokines/chemokines related to immune cell differentiation, cell survival, proliferation, angiogenesis and apoptosis in pooled esophageal tissue from12 month old L2-IL1B mice on Chow (n=4) or HFD (n=6). (C) Treatment with serum from L2-IL1B mice on HFD induces proliferation of 3D mouse BE organoids from L2-IL1B mice (Serum was collected and pooled from L2-IL1B mice maintained on Chow or HFD (n=3)). (D) qRT-PCR of CXCL1/KCin SCJ of L2-IL1B mice on HFD at 12 months (n=6). (E) a-SMA+ staining in L2-IL1B mice on HFD (n=6). (F) IL8 concentration in supernatant from esophageal squamous (Het), BE (QH) and EAC cell lines OE33 (n=3). (G) IL8 concentration in tissue conditioned medium from human normal esophagus, oesophagitis, BE and EAC. (n=10). NCM-normal conditioned medium, OCM-oesophagitis, BCM-BE, and TCM-EAC. Data are represented as mean ± SEM (****p<0.0001, ***p<0.001, **p<0.01, *p<0.05) For (C,D) 2 way ANOVA with Sidak-Holm post-hoc was used, for (E,F) 1 way Anova with Tukey post-hoc was used. (G) used a Kruskal-Wallis test against NCM and Dunns post-ho . L2=L2-IL-1β, WT=wildtype, HFD=High fat diet

Figure 3. IL8 is one of the key cytokines that accelerates esophageal dysplasia in HFD mice.

(A) Representative macroscopic pictures and Haematoxylin & Eosin (H&E) staining and (B) macroscopic tumor score in L2-IL1B/IL8Tg mice (n=10). (C) metaplasia and (D) dysplasia score in mice (n=8, mean ± SD). (E) Ki67 (F) PAS and (G) a-SMA^{+} staining in L2-IL1B/IL8Tg mice (n=6, mean ± SEM). (H) Gene Set Enrichment Analysis (GSEA): Differential expression between (i) WT HFD and Chow mice, (ii) L2-IL1B and WT Chow mice and (iii) L2-IL1B HFD and Chow mice (n=3) and analyzed with IL8 gene set, generated by utilizing gene expression data from L2-IL1B/IL8Tg mice and L2-IL-1β mice (n=3, mean ± SEM). (I) 3D mouse BE organoids from L2-IL1B/IL8Tg mice co-cultured with human lean or obese serum (pooled from 10 patients) for 48 hours. (****p<0.0001, ***p<0.001, **p<0.01, *p<0.05) For (B-D) a 2 way Anova with Sidak-Holm post-hoc was used. (E-G) use a 1 way Anova with Tukey post-hoc. (I) uses a t-test. L2=L2-IL-1β, L2/IL8Tg=L2-IL-1β/IL8Tg, HFD=High fat diet.

Figure 4. HFD induces a specific immune response with neutrophils infiltration and NK cells reduction.

(A) FACS of neutrophils, immature myeloid cells (IMC) and NK cells in the esophagus of HFD mice at 12 months (n=9-11). (B) IHC of neutrophils (Ly6G), immature myeloid cells (Ly6C) and macrophages (F4/80) in the squamous epithelium in 10 low power fields (n=3). (C) FACS of neutrophils in esophagus of L2-IL1B/IL8Tg mice (n=5-8). (D) IHC of neutrophils (Ly6G) in L2-IL1B/IL8Tgmice (n=3). (E) Cxcr2 expression and (F) score in the esophagus of L2-IL1B mice on HFD and in L2-IL1B/IL8Tg mice (n=8). (G) Proliferation of BE organoids of L2-IL1B mice co-cultured with neutrophils from the spleens of 9-12 months old L2-IL-1 β mice including a representative image of the organoids (n=3). (H) and (I) Cytokine arrays of BE organoid co-culture with neutrophils. Data are represented as mean ± SEM (*p<0.05) (A-C) use t-tests. (D,F) uses a 1 way Anova with Tukey post-hoc. (G) is a repeated measure 2 way Anova with Tukey post-hoc. L2=L2-IL-1β, L2/IL8Tg=L2-IL-1β/IL8Tg, HFD=High fat diet.

Figure 5. The esophageal inflammatory niche recruits SCJ progenitor cells

(A) CXCR2 expression in BE in L2-IL1B mice on HFD and in L2-IL1B/IL8Tg mice and germfree L2-IL1B mice (n=4-8). GSEAs for (B) a mouse epithelial (cancer) stem cells gene signatures comparing L2-IL1B HFD vs. L2-IL1B Chow and L2-IL1B/IL8Tg vs. L2-IL1B Chow or a (C) human migratory cancer cell gene signature. (D) ISH for Lgr5+ progenitor cells at the SCJ in the BE region in L2-IL-1B mice on HFD and in L2-IL1B/IL8Tg mice compared to germfree L2-IL1B mice (n=5-7). (E) ISH show co-expression of $Lgr5^{+}$ (brown) and CXCR2 (red) progenitor cells. (F) Crypt fission in L2-IL1B HFD mice and L2-IL1B/IL8Tg mice. Data are represented as mean ± SEM (*p<0.05). L2=L2-IL-1β, L2/IL8Tg=L2-IL-1β/IL8Tg, HFD=High fat diet.

Figure 6. The effect of HFD on the intestinal microbiome.

(A) Weighted Unifrac plot shows β-diversity after 16S-rRNA gene-sequencing of feces from L2-IL1B and WT mice on Chow (n=10), Control (n=6) and HFD (n=10) at the age of 6 months. (B) Ratio of the phylum Firmicutes to Bacteroidetes calculated after 16s-rRNA sequencing. Left: WT and L2-IL1B mice. Right: patient cytosponge samples (Control n=20, BE n=24, HGD n=23). (C) Representative H&E staining of SCJ and (D) Quantification of inflammation, metaplasia, dysplasia scores and goblet cell ratio in germfree (n=8, age 14 months, mean ± SD) and conventional L2-IL1B mice (n=16, age 11.5-16.5 months). (E) Representative pictures and quantification of IHC of neutrophils in the squamous epithelium in 10 low power fields (Ly6G) and IMCs (Ly6C) in germfree L2-IL1B mice (Germfree n=8, L2-IL1B-Chow n=3, L2-IL1B-HFD n=4). Groups with grey background are same mice as in Figure 4B. (F) Dysplasia score of L2-IL1B mice on control diet exposed to the old bedding of HFD L2-IL-1β mice (G) Principal component analysis of all significantly regulated KEGG pathways of the microbiome of WT (left) and L2-IL1B mice (right) at 6 months. (H) KEGG pathways of the microbiome in WT vs L2-IL1B mice on Chow (n=10 each), Control (n=6 each) and HFD (n=10 each) predicting the microbiomes function with PICRUSt. (I) KEGG pathway prediction of LPS synthesis. (J and K) GSEAs show an enrichment of mouse derived LPS response and TLR signaling in L2-IL1B-HFD mice. Data are represented as mean ± SEM. *p<0.05, **p<0.01 ***p<0.001. (B,E,F) used a 1-way ANOVA with Tukey post-hoc testing. For (D) a t-test was used. L2=L2-IL-1β, wt=wildtype, HFD=High fat diet.

References

1. Quante M, Graham TA, Jansen M. Insights into the Pathophysiology of Esophageal Adenocarcinoma. Gastroenterology 2017.
2. di Pietro M, Alzoubaidi D, Fitzgerald RC. Barrett's esophagus and cancer risk: how research advances can impact clinical practice. Gut Liver 2014;8:356-70.
3. Maret-Ouda J, El-Serag HB, Lagergren J. Opportunities for Preventing Esophageal Adenocarcinoma. CancerPrevRes(Phila) 2016;9:828-834.
4. El-Serag HB, Hashmi A, Garcia J, et al. Visceral abdominal obesity measured by CT scan is associated with an increased risk of Barrett's oesophagus: a case-control study. Gut 2014;63:220-9.
5. Nguyen TH, Thrift AP, Ramsey D, et al. Risk factors for Barrett's esophagus compared between African Americans and non-Hispanic Whites. Am J Gastroenterol 2014;109:1870-80.
6. Goodwin PJ, Chlebowski RT. Obesity and Cancer: Insights for Clinicians. J Clin Oncol 2016;34:4197-4202.
7. Thrift AP, Hilal J, El-Serag HB. Metabolic syndrome and the risk of Barrett's oesophagus in white males. Aliment Pharmacol Ther 2015;41:1182-9.
8. Tabung FK, Liu L, Wang W, et al. Association of Dietary Inflammatory Potential With Colorectal Cancer Risk in Men and Women. JAMAOncol 2018.
9. David LA, Maurice CF, Carmody RN, et al. Diet rapidly and reproducibly alters the human gut microbiome. Nature 2014;505:559-63.
10. **Beyaz S, Mana MD, Roper J**, et al. High-fat diet enhances stemness and tumorigenicity of intestinal progenitors. Nature 2016;531:53-8.
11. Ericksen RE, Rose S, Westphalen CB, et al. Obesity accelerates Helicobacter felis-induced gastric carcinogenesis by enhancing immature myeloid cell trafficking and TH17 response. Gut 2013.
12. Singh S, Sharma AN, Murad MH, et al. Central adiposity is associated with increased risk of esophageal inflammation, metaplasia, and adenocarcinoma: a systematic review and meta-analysis. Clin Gastroenterol Hepatol 2013;11:1399-1412 e7.
13. **Schulz MD, Atay C, Heringer J**, et al. High-fat-diet-mediated dysbiosis promotes intestinal carcinogenesis independently of obesity. Nature 2014;514:508-12.
14. Quante M, Bhagat G, Abrams JA, et al. Bile Acid and Inflammation Activate Gastric Cardia Stem Cells in a Mouse Model of Barrett-Like Metaplasia. Cancer Cell 2012;21:36-51.
15. **Asfaha S, Dubeykovskiy AN**, Tomita H, et al. Mice that express human interleukin-8 have increased mobilization of immature myeloid cells, which exacerbates inflammation and accelerates colon carcinogenesis. Gastroenterology 2013;144:155-66.
16. Bolze F, Rink N, Brumm H, et al. Characterization of the melanocortin-4-receptor nonsense mutation W16X in vitro and in vivo. Pharmacogenomics J 2013;13:80-93.
17. Lertpiriyapong K, Whary MT, Muthupalani S, et al. Gastric colonisation with a restricted commensal microbiota replicates the promotion of neoplastic lesions by diverse intestinal microbiota in the Helicobacter pylori INS-GAS mouse model of gastric carcinogenesis. Gut 2014;63:54-63.
18. Farooqi IS, Yeo GS, Keogh JM, et al. Dominant and recessive inheritance of morbid obesity associated with melanocortin 4 receptor deficiency. J Clin Invest 2000;106:271-9.
19. Fitzgerald RC, Abdalla S, Onwuegbusi BA, et al. Inflammatory gradient in Barrett's oesophagus: implications for disease complications. Gut 2002;51:316-22.
20. Catusse J, Liotard A, Loillier B, et al. Characterization of the molecular interactions of interleukin-8 (CXCL8), growth related oncogen alpha (CXCL1) and a non-peptide antagonist (SB 225002) with the human CXCR2. Biochem Pharmacol 2003;65:813-21.
21. Spiegel A, Brooks MW, Houshyar S, et al. Neutrophils Suppress Intraluminal NK Cell-Mediated Tumor Cell Clearance and Enhance Extravasation of Disseminated Carcinoma Cells. Cancer Discov 2016;6:630-49.
22. **Wang X, Ouyang H, Yamamoto Y**, et al. Residual embryonic cells as precursors of a Barrett's-like metaplasia. Cell 2011;145:1023-35.
23. Cancer Genome Atlas Research N, Analysis Working Group: Asan U, Agency BCC, et al. Integrated genomic characterization of oesophageal carcinoma. Nature 2017;541:169-175.
24. O'Neil A, Petersen CP, Choi E, et al. Unique Cellular Lineage Composition of the First Gland of the Mouse Gastric Corpus. J Histochem Cytochem 2017;65:47-58.
25. Elliott DR, Walker AW, O'Donovan M, et al. A non-endoscopic device to sample the oesophageal microbiota: a case-control study. Lancet Gastroenterol Hepatol 2017;2:32-42.

26. Kubeck R, Bonet-Ripoll C, Hoffmann C, et al. Dietary fat and gut microbiota interactions determine diet-induced obesity in mice. Mol Metab 2016;5:1162-1174.
27. **Langille MG, Zaneveld J**, Caporaso JG, et al. Predictive functional profiling of microbial communities using 16S rRNA marker gene sequences. Nat Biotechnol 2013;31:814-21.
28. Abrams JA, Sharaiha RZ, Gonsalves L, et al. Dating the rise of esophageal adenocarcinoma: analysis of Connecticut Tumor Registry data, 1940-2007. Cancer Epidemiol Biomarkers Prev 2011;20:183-6.
29. Rieder F, Bianchini P, Harnett K, et al. Inflammatory mediators in gastroesophageal reflux disease: impact on esophageal motility, fibrosis, and carcinogenesis. American Physiological Society 2010;298:G571-G581.
30. Hardikar S, Onstad L, Song X, et al. Inflammation and oxidative stress markers and esophageal adenocarcinoma incidence in a Barrett's esophagus cohort. Cancer Epidemiol Biomarkers Prev 2014.
31. Xing F, Saidou J, Watade K. Cancer associated fibroblasts (CAFs) in tumor microenvironment. Front Biosci. 2011;15:166-179.
32. Shrivastava MS, Hussain Z, Giricz O, et al. Targeting chemokine pathways in esophageal adenocarcinoma. Cell Cycle 2014;13:3320-7.
33. Cook MB, Barnett MJ, Bock CH, et al. Prediagnostic circulating markers of inflammation and risk of oesophageal adenocarcinoma: a study within the National Cancer Institute Cohort Consortium. Gut 2018.
34. Garcia JM, Splenser AE, Kramer J, et al. Circulating inflammatory cytokines and adipokines are associated with increased risk of Barrett's esophagus: a case-control study. Clin Gastroenterol Hepatol 2014;12:229-238 e3.
35. Thrift AP, Garcia JM, El-Serag HB. A multibiomarker risk score helps predict risk for Barrett's esophagus. Clin Gastroenterol Hepatol 2014;12:1267-71.
36. Bhattacharyya S, Borthakur A, Pant N, et al. Bcl10 mediates LPS-induced activation of NF-kappaB and IL-8 in human intestinal epithelial cells. Am J Physiol Gastrointest Liver Physiol 2007;293:G429-37.
37. Adler BJ, Green DE, Pagnotti GM, et al. High fat diet rapidly suppresses B lymphopoiesis by disrupting the supportive capacity of the bone marrow niche. PLoS One 2014;9:e90639.
38. Coffelt SB, Wellenstein MD, de Visser KE. Neutrophils in cancer: neutral no more. Nat Rev Cancer 2016;16:431-46.
39. Waight JD, Hu Q, Miller A, et al. Tumor-derived G-CSF facilitates neoplastic growth through a granulocytic myeloid-derived suppressor cell-dependent mechanism. PLoS One 2011;6:e27690.
40. Casbon A-J, Reynaud D, Park C, et al. Invasive breast cancer reprograms early myeloid differentiation in the bone marrow to generate immunosuppressive neutrophils. Proc Natl Acad Sci USA 2015;112:E566-575.
41. **Xu B, Chen L**, Li J, et al. Prognostic value of tumor infiltrating NK cells and macrophages in stage II+III esophageal cancer patients. Oncotarget 2016;7:74904-74916.
42. **Quail DF, Olson OC**, Bhardwaj P, et al. Obesity alters the lung myeloid cell landscape to enhance breast cancer metastasis through IL5 and GM-CSF. Nat Cell Biol 2017;19:974-987.
43. Alexeev V, Salas-Alanis JC, Palisson F, et al. Pro-inflammatory chemokines and cytokines dominate the blister fluid molecular signature in epidermolysis bullosa patients and affect leukocyte and stem cell migration. J Invest Dermatol 2017.
44. Ray K. High-fat diet influences intestinal stem cell biology. Nature Reviews Gastroenterology& Hepatology 2016;13:250-251.
45. Duggan C, Onstad L, Hardikar S, et al. Association between markers of obesity and progression from Barrett's esophagus to esophageal adenocarcinoma. Clin Gastroenterol Hepatol 2013;11:934-43.
46. Wu GD, Chen J, Hoffmann C, et al. Linking long-term dietary patterns with gut microbial enterotypes. Science 2011;334:105-8.
47. Kim HJ, Li H, Collins JJ, et al. Contributions of microbiome and mechanical deformation to intestinal bacterial overgrowth and inflammation in a human gut-on-a-chip. Proc Natl Acad Sci USA 2016;113:E7-15.
48. **Schueller K, Riva A, Pfeiffer S**, et al. Members of the Oral Microbiota Are Associated with IL-8 Release by Gingival Epithelial Cells in Healthy Individuals. Front Microbiol 2017;8:416.
49. Sun L, Xie C, Wang G, et al. Gut microbiota and intestinal FXR mediate the clinical benefits of metformin. Nat Med 2018;24:1919-1929.
50. Snider EJ, Compres G, Freedberg DE, et al. Barrett's esophagus is associated with a distinct oral microbiome. Clin Transl Gastroenterol 2018;9:135.

51. Yang L, Lu X, Nossa CW, et al. Inflammation and intestinal metaplasia of the distal esophagus are associated with alterations in the microbiome. Gastroenterology 2009;137:588-97.
52. Ley RE, Turnbaugh PJ, Klein S, et al. Microbial ecology: Human gut microbes associated with obesity. Nature 2006;444:1022-1023.
53. Weber D, Hiergeist A, Weber M, et al. Detrimental effect of broad-spectrum antibiotics on intestinal microbiome diversity in patients after allogeneic stem cell transplantation: Lack of commensal sparing antibiotics. Clin Infect Dis 2018.

Figure 1:

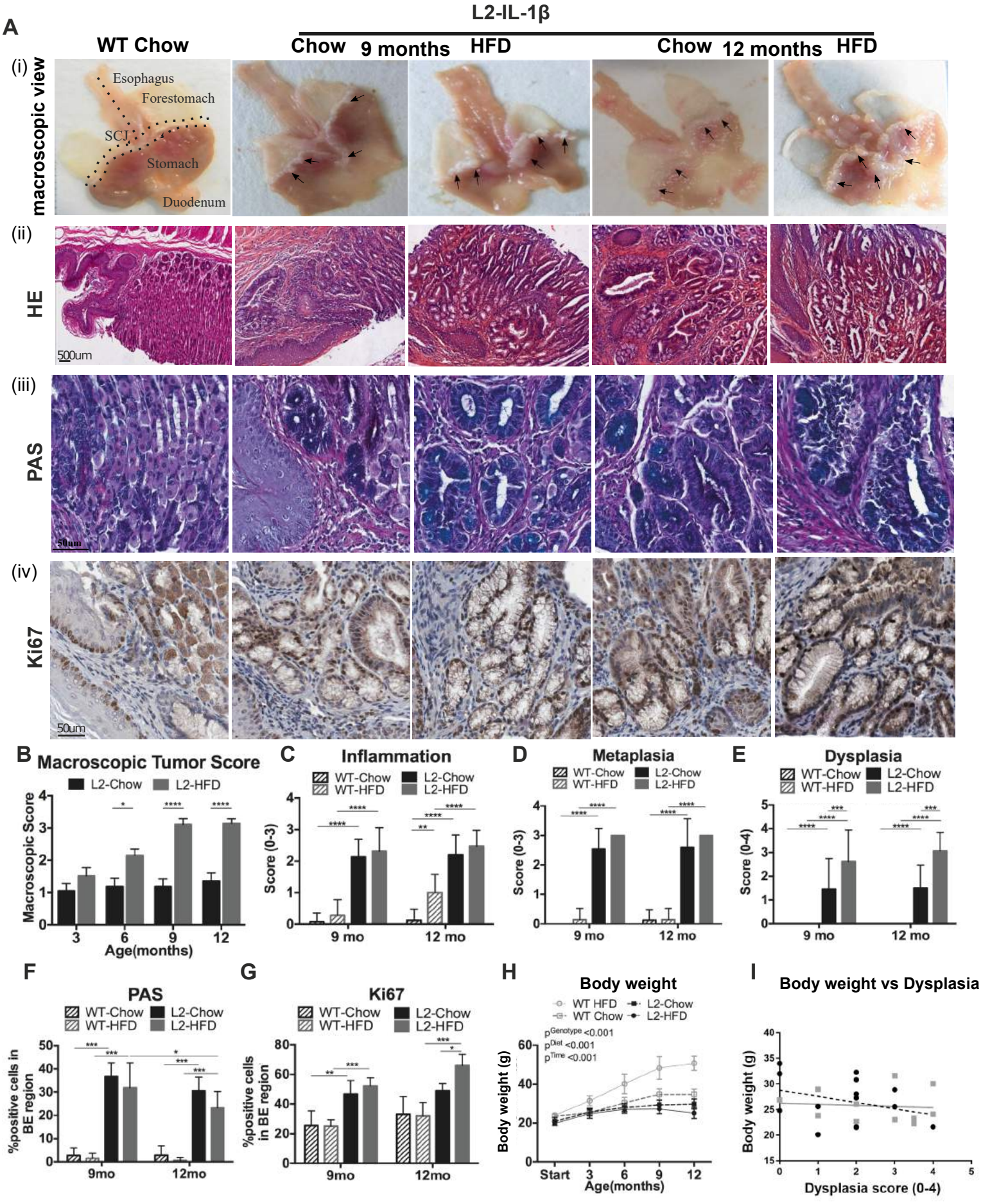
A
L2-IL-1β
WT Chow
Chow 9 months HFD
Chow 12 months HFD
(i) macroscopic view
Esophagus
Forestomach
SCJ
Stomach
Duodenum
(ii) HE
500um
(iii) PAS
50um
(iv) Ki67
50um
B Macroscopic Tumor Score
L2-Chow
L2-HFD
Macroscopic Score
Age(months)
C Inflammation
WT-Chow
WT-HFD
L2-Chow
L2-HFD
Score (0-3)
9 mo
12 mo
D Metaplasia
Score (0-3)
E Dysplasia
Score (0-4)
F PAS
%positive cells in BE region
9mo
12mo
G Ki67
H Body weight
WT HFD
WT Chow
L2-Chow
L2-HFD
Body weight (g)
Start
Age(months)
I Body weight vs Dysplasia
Dysplasia score (0-4)

Figure 2:

A

L2-HFD v. L2-Chow

Up-regulated	Symbol	Description	FC	P.Value
Cytokines & their receptors	Il1b	interleukin 1 beta	2.8931	0.0191
	Il17c	interleukin 17C	2.2093	0.0098
	Il2ra	interleukin 2 receptor, alpha chain	1.6505	0.0036
	Csf1r	colony stimulating factor 1 receptor	1.5206	0.075
	Wnt2b	wingless-type MMTV integration site family, member 2B	1.7256	0.0078
	Angpt2	angiopoietin 2	1.9333	0.0108
Chemokines & their receptors	Cxcl13	chemokine (C-X-C motif) ligand 13	3.613	0.0226
	Cxcr4	chemokine (C-X-C motif) receptor 4	1.8898	0.0073
	Ccl2	chemokine (C-C motif) ligand 2	2.6368	0.0366
	Ccl7	chemokine (C-C motif) ligand 7	2.4657	0.0148
	Ccl11	chemokine (C-C motif) ligand 11	2.2577	0.0024
	Ccr5	chemokine (C-C motif) receptor 5	1.8987	0.0325
	Ccr2	chemokine (C-C motif) receptor 2	1.8705	0.0208
	Ccl8	chemokine (C-C motif) ligand 8	1.8153	0.0184
	Ccr7	chemokine (C-C motif) receptor 7	1.7321	0.0289
	Ccl9	chemokine (C-C motif) ligand 9	1.5162	0.0537
Extracellular enzymes/ molecules	Mmp7	matrix metallopeptidase 7	3.5151	0.0132
	Mmp10	matrix metallopeptidase 10	1.8903	0.0464
	Mmp25	matrix metallopeptidase 25	1.5596	0.0411
	Mmp12	matrix metallopeptidase 12	1.5577	0.0238
Transcription, translation & RNA processing	Hspa1a	heat shock protein 1A	2.1531	0.0116
	Hspa1b	heat shock protein 1B	1.7076	0.0227
Cell viability	Igf1	insulin-like growth factor 1	1.5851	0.0283
	Igfbp4	insulin-like growth factor binding protein 4	1.696	0.006
Receptors & cell adhesion/ signaling	Tlr13	toll-like receptor 13	1.8489	0.0262
	Tlr8	toll-like receptor 8	1.691	0.0151
	Ctsk	cathepsin K	1.9414	0.0093
	Mrc1	mannose receptor, C type 1	2.4725	0.0097
	Vcam1	vascular cell adhesion molecule 1	1.5512	0.026
Inflammatory cytokine & receptors	TNF	Tumor necrosis factor	1.5948	0.0461
	Tlr13	Toll-like receptor 13	1.8488	0.0262
	Tlr8	Toll-like receptor 8	1.6910	0.0153
Intracellular transport	Vim	vimentin	1.655	0.0301
	Itga4	integrin alpha 4	1.5864	0.0315
	Ctsl	cathepsin L	1.4991	0.0553

L2-HFD v. L2Chow

Down-regulated	Symbol	Description	FC	P.Value
Cytokines & their receptors	Il20ra	interleukin 20 receptor, alpha	0.594	0.049
	Wnt7b	wingless-type MMTV integration site family, member 7B	0.6538	0.0209
Extracellular enzymes/ molecules	Krt7	keratin 7	0.6223	0.021
	Muc2	mucin 2	0.4981	0.0274
Cell viability	Egf	epidermal growth factor	0.5443	0.0076

B

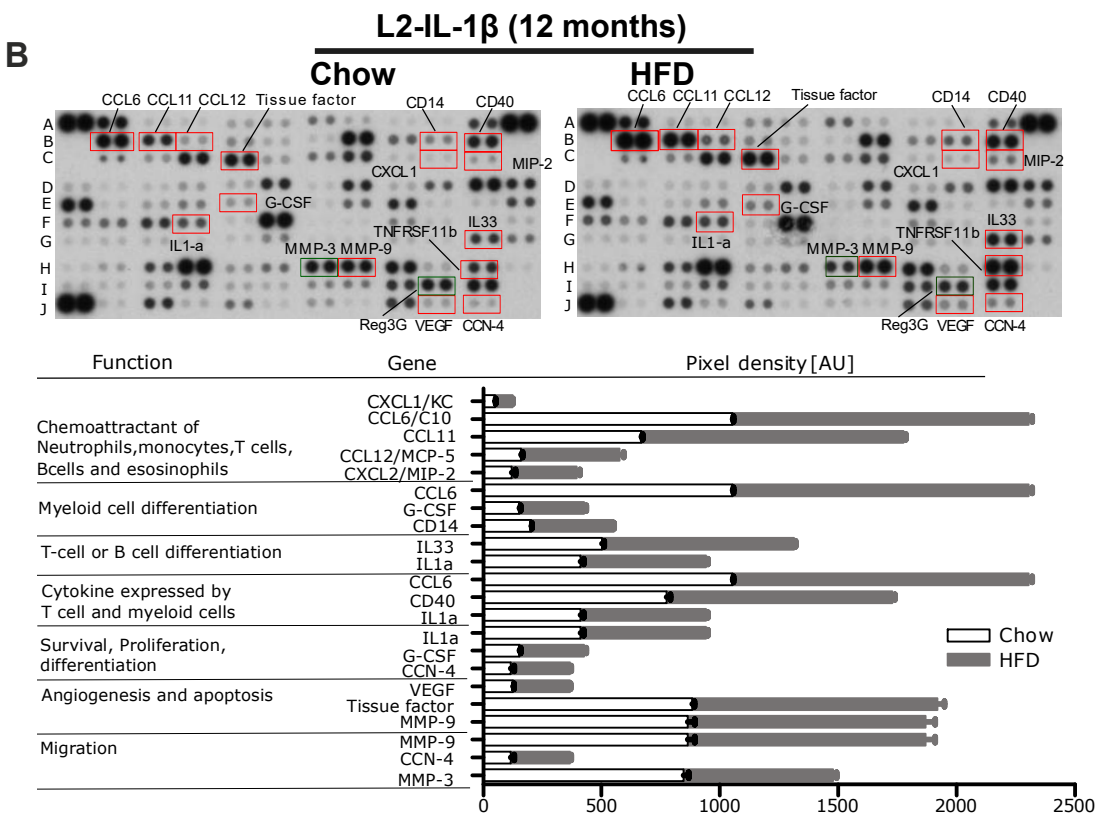

C

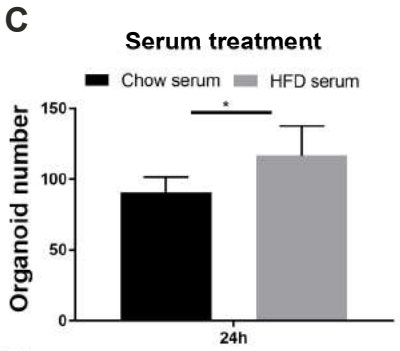

D

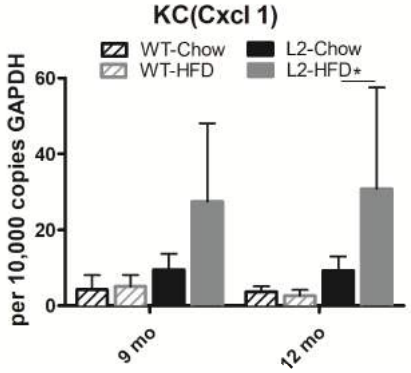

E

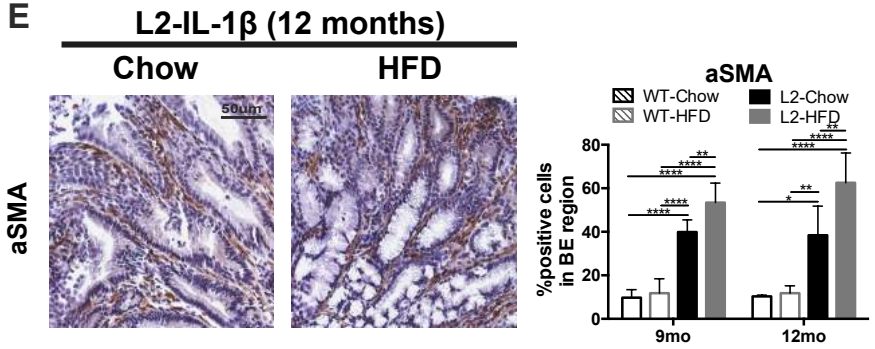

F

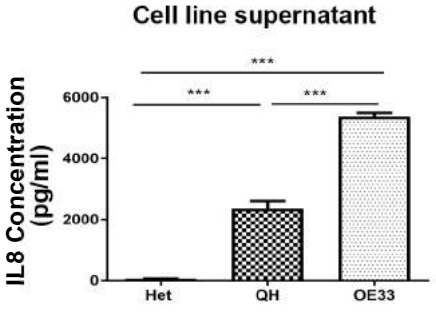

G

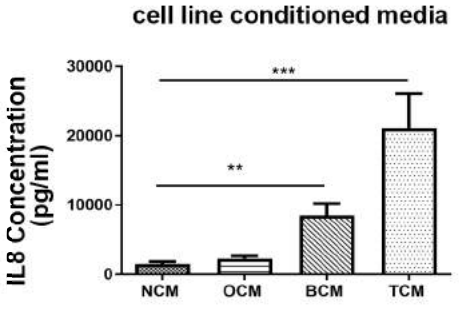

Figure 3:

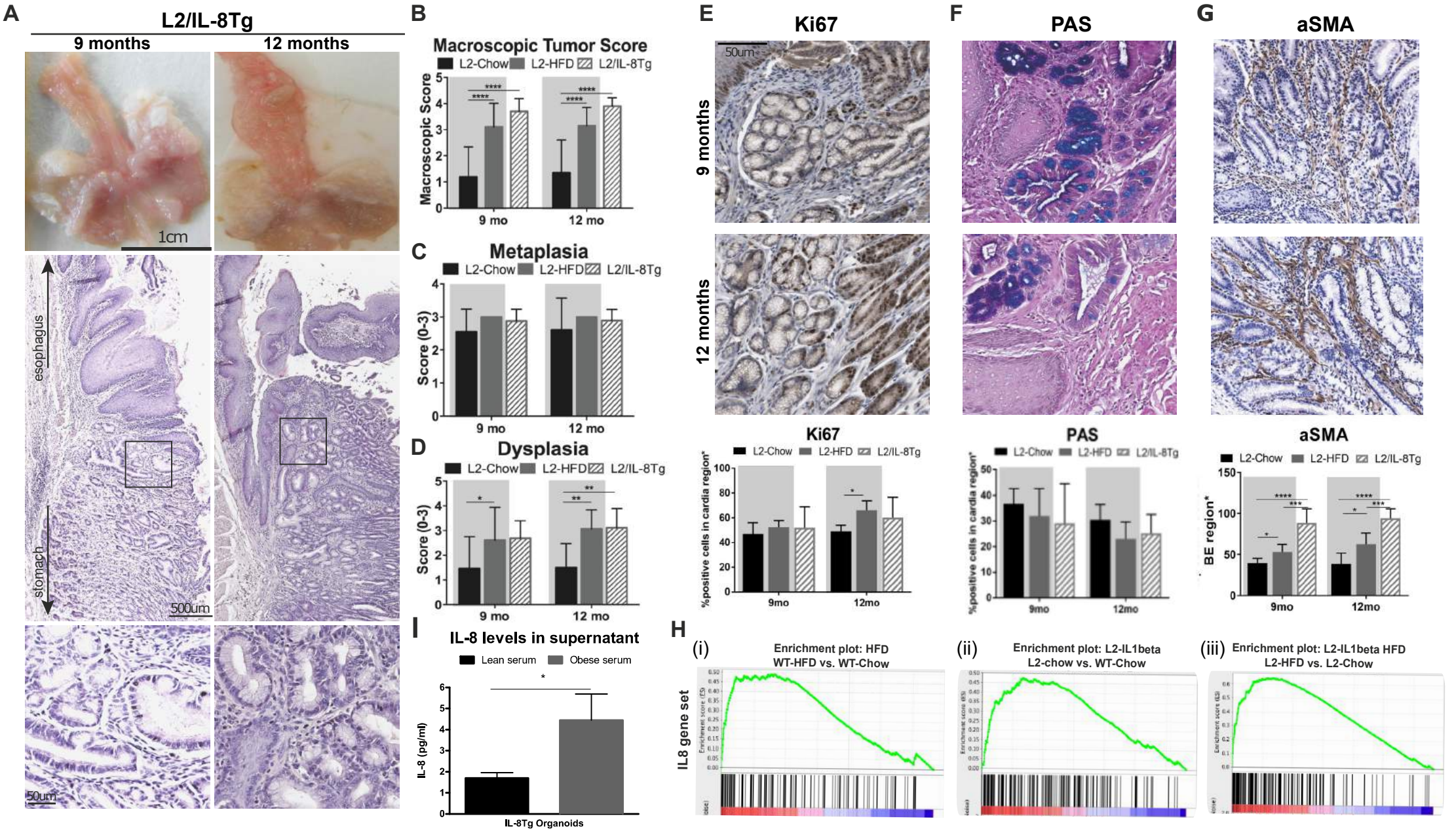
A
L2/IL-8Tg
9 months
12 months
1cm
esophagus
stomach
500um
50um
B
Macroscopic Tumor Score
L2-Chow L2-HFD L2/IL-8Tg
Macroscopic Score
9 mo
12 mo
C
Metaplasia
L2-Chow L2-HFD L2/IL-8Tg
Score (0-3)
9 mo
12 mo
D
Dysplasia
L2-Chow L2-HFD L2/IL-8Tg
Score (0-3)
9 mo
12 mo
I
IL-8 levels in supernatant
Lean serum Obese serum
IL-8 (pg/ml)
IL-8Tg Organoids
E
Ki67
50um
9 months
12 months
Ki67
L2-Chow L2-HFD L2/IL-8Tg
%positive cells in cardia region*
9mo
12mo
F
PAS
PAS
L2-Chow L2-HFD L2/IL-8Tg
%positive cells in cardia region*
9mo
12mo
G
aSMA
aSMA
L2-Chow L2-HFD L2/IL-8Tg
BE region*
9mo
12mo
H
IL8 gene set
(i)
Enrichment plot: HFD
WT-HFD vs. WT-Chow
(ii)
Enrichment plot: L2-IL1beta
L2-chow vs. WT-Chow
(iii)
Enrichment plot: L2-IL1beta HFD
L2-HFD vs. L2-Chow

Figure 4:

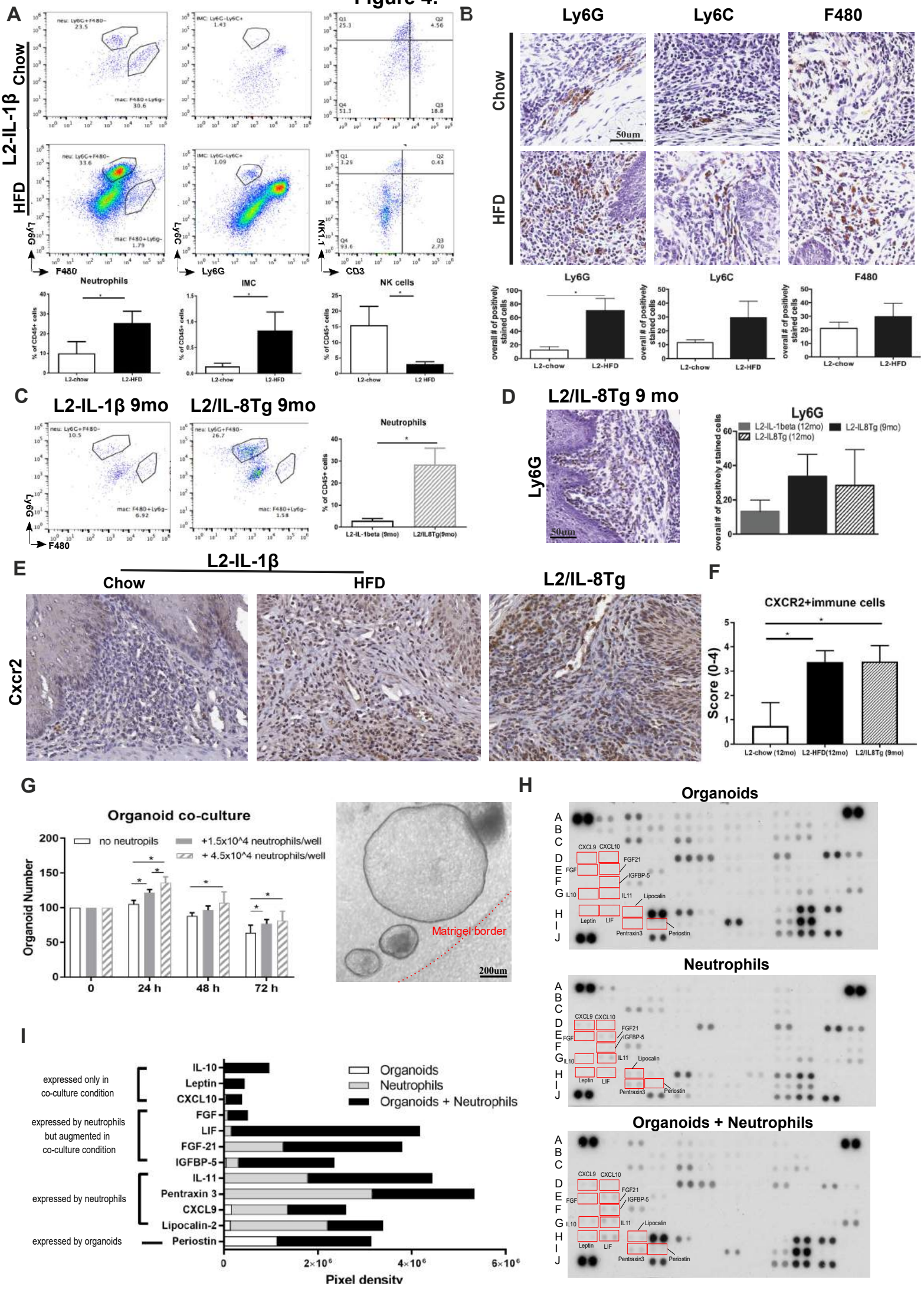
A
Chow
HFD
L2-IL-1β
F480
Ly6G
CD3
NK1.1
Neutrophils
IMC
NK cells
% of CD45+ cells
L2-chow
L2-HFD
B
Ly6G
Ly6C
F480
Chow
HFD
50um
overall # of positively stained cells
C
L2-IL-1β 9mo
L2/IL-8Tg 9mo
Neutrophils
L2-IL-1beta (9mo)
L2/IL8Tg(9mo)
D
L2/IL-8Tg 9 mo
Ly6G
L2-IL-1beta (12mo)
L2-IL8Tg (12mo)
L2-IL8Tg (9mo)
E
L2-IL-1β
Chow
HFD
L2/IL-8Tg
Cxcr2
F
CXCR2+immune cells
Score (0-4)
L2-chow (12mo)
L2-HFD(12mo)
L2/IL8Tg (9mo)
G
Organoid co-culture
no neutrophils
+1.5x10^4 neutrophils/well
+ 4.5x10^4 neutrophils/well
Organoid Number
0
24 h
48 h
72 h
Matrigel border
200um
H
Organoids
Neutrophils
Organoids + Neutrophils
CXCL9
CXCL10
FGF21
FGF
IGFBP-5
IL10
IL11
Lipocalin
Leptin
LIF
Pentraxin3
Periostin
I
expressed only in co-culture condition
expressed by neutrophils but augmented in co-culture condition
expressed by neutrophils
expressed by organoids
IL-10
Leptin
CXCL10
FGF
LIF
FGF-21
IGFBP-5
IL-11
Pentraxin 3
CXCL9
Lipocalin-2
Periostin
Organoids
Neutrophils
Organoids + Neutrophils
Pixel density

Figure 5:

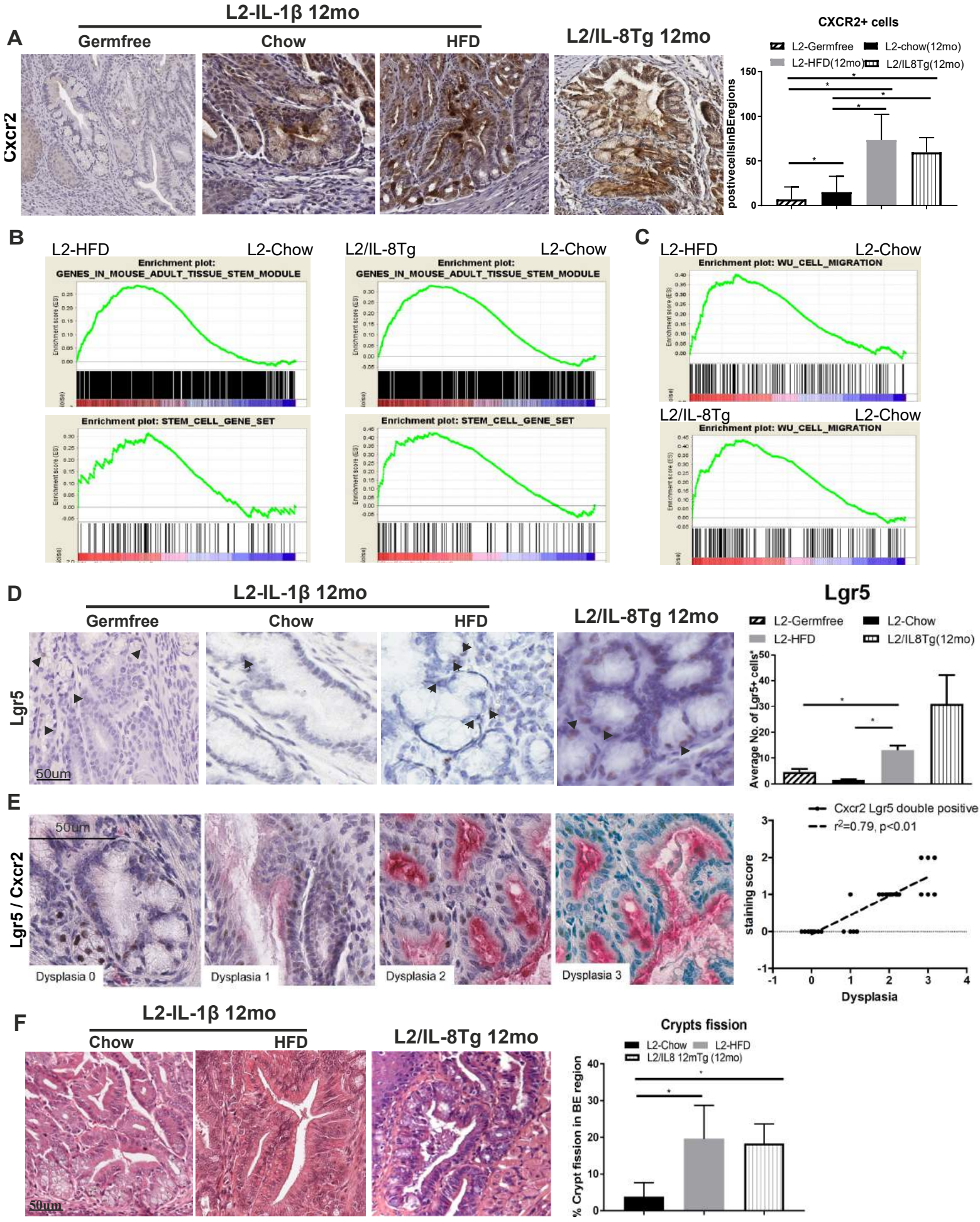
A
L2-IL-1β 12mo
Germfree
Chow
HFD
L2/IL-8Tg 12mo
Cxcr2
CXCR2+ cells
L2-Germfree
L2-chow(12mo)
L2-HFD(12mo)
L2/IL8Tg(12mo)
postivecellsinBEregions
B
L2-HFD
L2-Chow
L2/IL-8Tg
Enrichment plot: GENES_IN_MOUSE_ADULT_TISSUE_STEM_MODULE
Enrichment plot: STEM_CELL_GENE_SET
C
Enrichment plot: WU_CELL_MIGRATION
D
Lgr5
50um
Average No. of Lgr5+ cells*
E
Lgr5 / Cxcr2
Dysplasia 0
Dysplasia 1
Dysplasia 2
Dysplasia 3
Cxcr2 Lgr5 double positive
r²=0.79, p<0.01
staining score
Dysplasia
F
Crypts fission
% Crypt fission in BE region
L2-Chow
L2-HFD
L2/IL8 12mTg (12mo)

Figure 6:

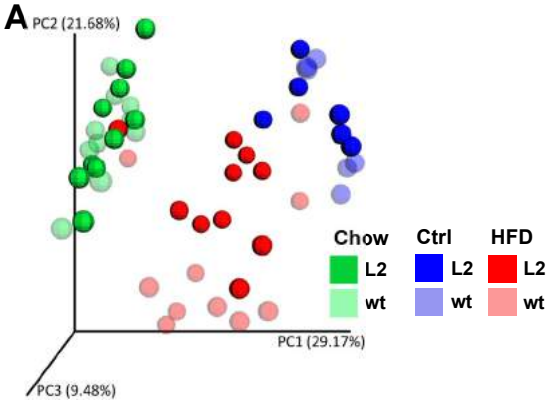
A
PC2 (21.68%)
PC1 (29.17%)
PC3 (9.48%)
Chow
L2
wt
Ctrl
L2
wt
HFD
L2
wt

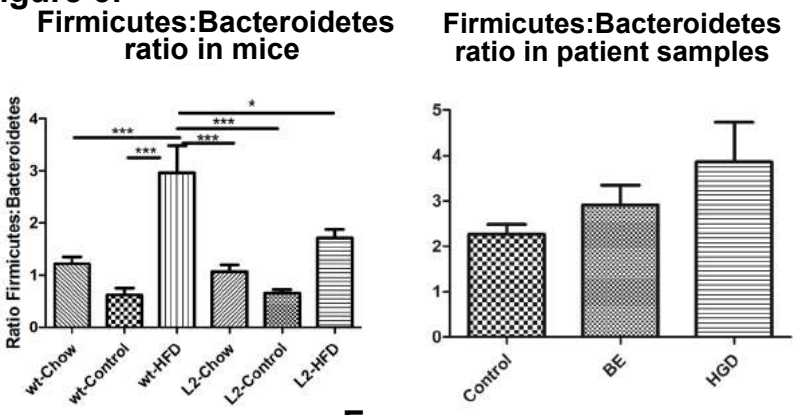
B
Firmicutes:Bacteroidetes ratio in mice
Ratio Firmicutes:Bacteroidetes
wt-Chow
wt-Control
wt-HFD
L2-Chow
L2-Control
L2-HFD
Firmicutes:Bacteroidetes ratio in patient samples
Control
BE
HGD

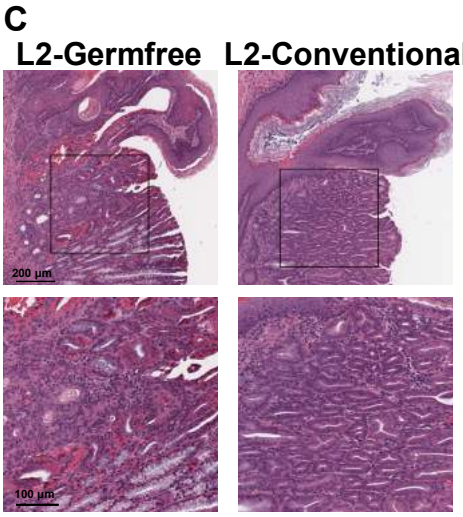
C
L2-Germfree
L2-Conventional
200 µm
100 µm

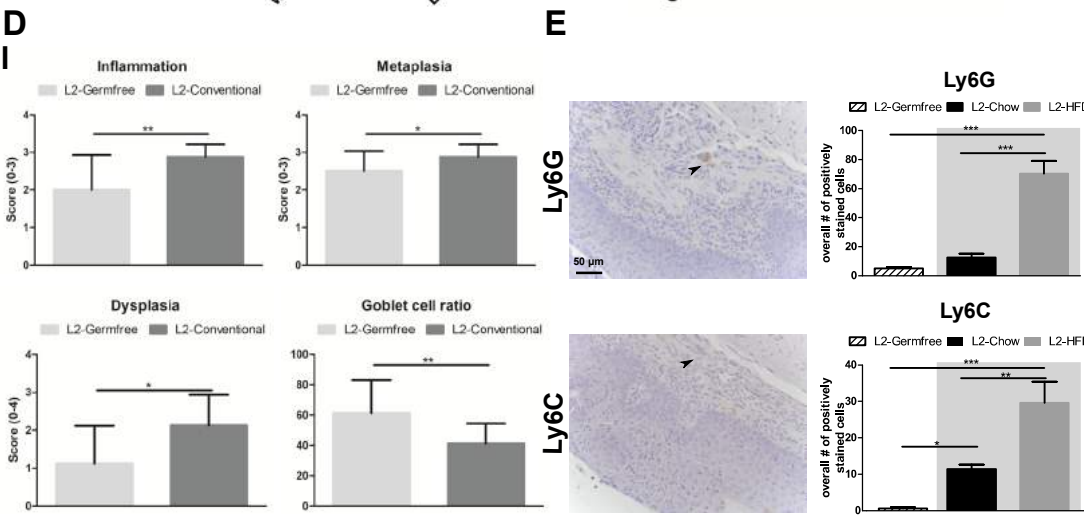
D
Inflammation
Metaplasia
Dysplasia
Goblet cell ratio
L2-Germfree
L2-Conventional
E
Ly6G
Ly6C
50 µm
L2-Germfree
L2-Chow
overall # of positively stained cells

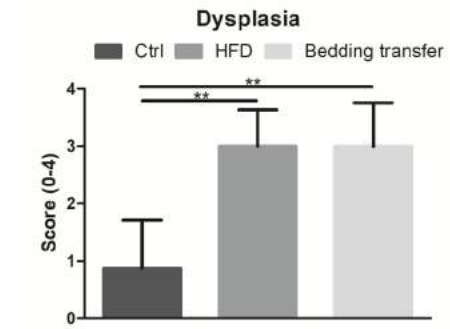
F
Dysplasia
Ctrl
HFD
Bedding transfer
Score (0-4)

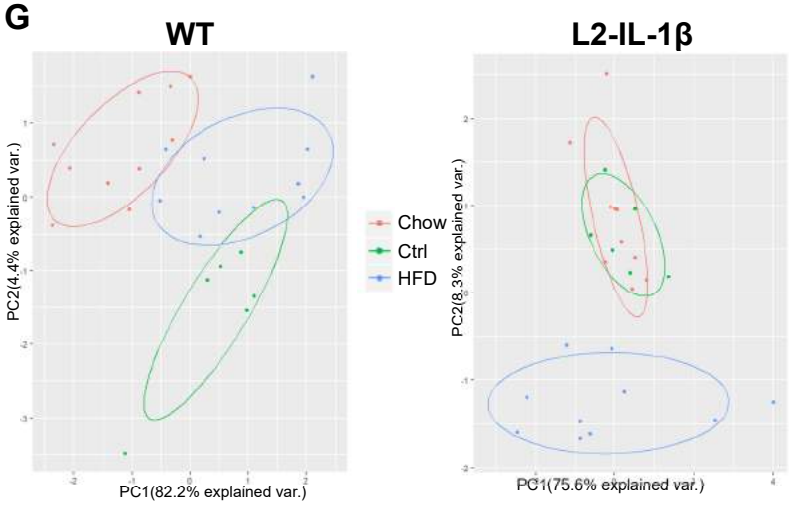
G
WT
L2-IL-1β
Chow
Ctrl
HFD
PC2(4.4% explained var.)
PC1(82.2% explained var.)
PC2(8.3% explained var.)
PC1(75.6% explained var.)

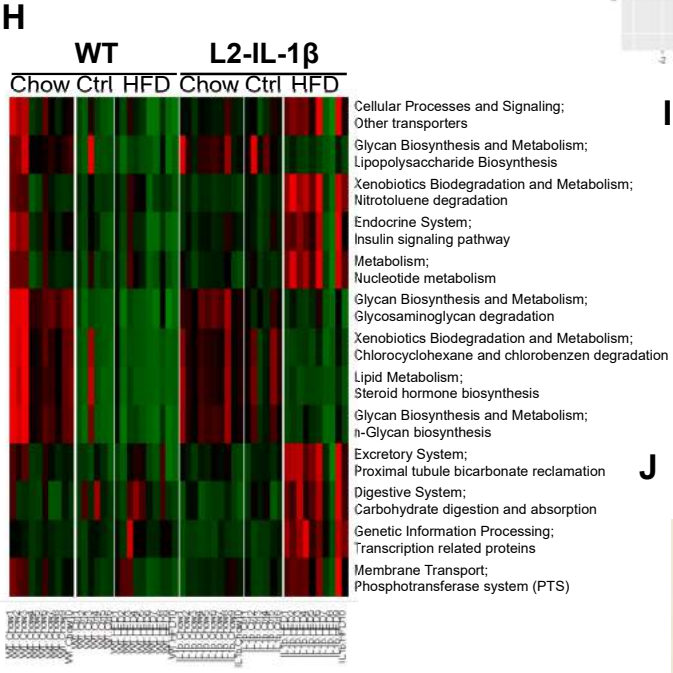
H
WT
L2-IL-1β
Chow Ctrl HFD Chow Ctrl HFD
Cellular Processes and Signaling; Other transporters
Glycan Biosynthesis and Metabolism; Lipopolysaccharide Biosynthesis
Xenobiotics Biodegradation and Metabolism; Nitrotoluene degradation
Endocrine System; Insulin signaling pathway
Metabolism; Nucleotide metabolism
Glycan Biosynthesis and Metabolism; Glycosaminoglycan degradation
Xenobiotics Biodegradation and Metabolism; Chlorocyclohexane and chlorobenzen degradation
Lipid Metabolism; Steroid hormone biosynthesis
Glycan Biosynthesis and Metabolism; n-Glycan biosynthesis
Excretory System; Proximal tubule bicarbonate reclamation
Digestive System; Carbohydrate digestion and absorption
Genetic Information Processing; Transcription related proteins
Membrane Transport; Phosphotransferase system (PTS)

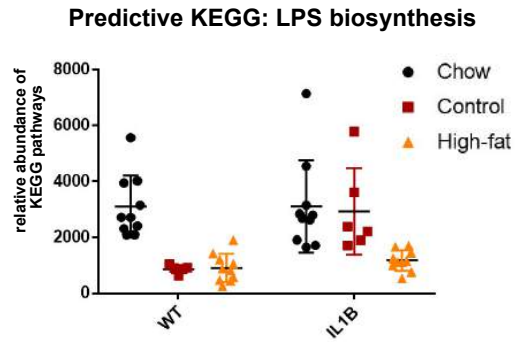
I
Predictive KEGG: LPS biosynthesis
relative abundance of KEGG pathways
Chow
Control
High-fat
WT
IL1B

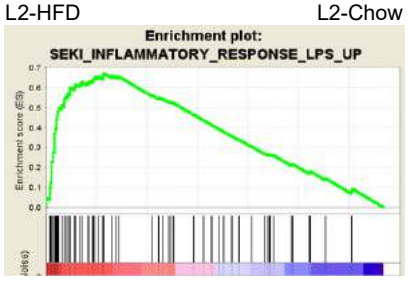
J
L2-HFD
L2-Chow
Enrichment plot:
SEKI_INFLAMMATORY_RESPONSE_LPS_UP

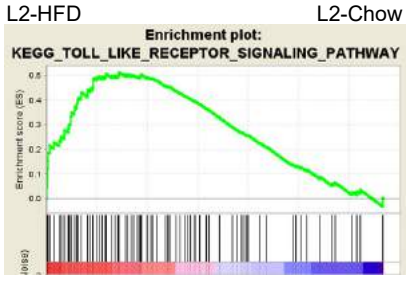
K
L2-HFD
L2-Chow
Enrichment plot:
KEGG_TOLL_LIKE_RECEPTOR_SIGNALING_PATHWAY

Need to Know

Background:

We investigated whether a high-fat diet and/or obesity contribute to progression of Barrett's esophagus (BE) to esophageal cancer in a mouse model and by studying esophageal tissues from patients with BE.

Findings:

We found a high-fat diet to promote esophageal dysplasia by altering the intestinal microbiome and promoting inflammation and stem cell expansion, independent of obesity.

Implications for Patient Care:

Patients with BE should be encouraged to avoid a high-fat diet.

Lay Summary:

In an inflammation induced mouse model of esophageal tumor development a diet rich in fat is leading to accelerated tumor growth in part caused by changes in the gut microbiome which induces an accelerated inflammatory microenvironment.

Supplement

High fat diet accelerates Barrett esophageal carcinogenesis by IL-8 dependent immune and stem cell responses through changes in gut microbiota

Supplementary Figure Legends

Supplementary Figure 1.

(A) Nutrient composition of the Chow and high fat diet. (B) Areas which are evaluated for the scoring of acroscopic lesion are highlighted in red (C) Representative images of WT HFD mice showing macroscopic imaging of the stomach and esophagus, HE, PAS and Ki67 staining (D) Scoring protocol for macroscopic lesions. SCJ and esophagus were evaluated for tumors based on size and coverage (E) Scoring for microscopic scoring of HE slides (F) Fat and lean mass in L2-IL-1β mice and wild type mice, data is presented as mean ± SEM (n=12). WT: wild type. HFD: High fat diet. L2-Chow: L2-IL-1β mice on Chow feeding. L2-HFD: L2-IL-1β mice on HFD feeding.

Supplementary Figure 2.

(A) Representative images of Mc4r^{het}, Mc4r^{ki}, L2-IL-1β/Mc4r^{het} and L2-IL-1β/Mc4r^{ki} stomach and HE sections.(B) Body weight until the age of 12 months of wildtype mice on a HFD and Mc4r^{ki} mice. (C) Fat mass of wiltype HFD mice and Mc4r^{ki} mice (D) Macroscopic tumor score of L2-IL-1β/Mc4r^{het} (n=3), L2-IL-1β/Mc4r^{ki} (n=4), L2-IL-1β Chow (n=10) and L2-IL-1β HFD (n=15) mice. Quantification of the inflammation (E), metaplasia (F) -, dysplasia (G) scores of L2-IL-1β/Mc4r^{het} (n=3, mean ± SD), L2-IL-1β/Mc4r^{ki} (n=4), L2-IL-1βChow (n=10) and L2-IL-1βHFD (n=15) mice. (H) Spleen to body mass ratio of Mc4r^{het}, Mc4r^{ki}, L2-IL-1β/Mc4r^{het} and L2-IL-1β/Mc4r^{ki} mice. (I) Spleen to body mass ratio calculated for WT and L2-IL-1β mice on Chow and HFD feeding (n=12 per group, mean ± SEM). WT: wild type. L2: L2-IL-1β mice HFD: High fat diet. Chow=regular lab chow. ** : p<0.01, ***: p<0.001, ****: p<0.0001 (D-G) Grey background within the graphs indicate that these are the same mice as in Figure 1A

Supplementary Figure 3.

(A) Shown are relevant enrichment plots comparing L2-IL-1β HFD with L2-IL-1β Chow fed mice if not indicated otherwise. All displayed GSEAs have a p-value of less than 0.01. (B) Quantitative Real-Time PCR of MMP3 and MMP7 in esophageal tissue lysates from L2-IL-1β HFD mice normalized to GAPDH (n=6). (C) Cytokine arrays of pooled serum from WT-Chow, WT-HD, L2-Chow and L2-HFD

mice. Data is presented as mean ± SEM HFD: High fat diet. L2-Chow: L2-IL-1β mice maintained on Chow diet. L2-HFD: L2-IL-1β mice on HFD feeding.

Supplementary Figure 4.

(A) Serum profiles of 19 lean patients and 20 obese patients. (B) Quantification of inflammation score in L2-IL-1β/IL-8Tg mice, presented as mean ± SD. Grey background within the graphs indicate that these are the same mice as in Figure 1A (C) IL-8 concentrations in serum from human esophagitis patients, BE patients, low grade (LGD) - high-grades dysplasia (HGD) patients, and EAC patients.(D) Correlations between body mass index (BMI) and IL8 concentration in serum. (E) Organoid growth from organoids derived from L2-IL-1β/IL-8Tg mice treated with either human lean serum or human obese serum (pooled from n=10 patients). Data is presented as mean ± SEM.

Supplementary Figure 5.

(A) Gating strategy for the FACS analysis of immune cells. (B) FACS analysis shows no significant increases in macrophages, $CD3^+CD4^+$ T helper cells, $CD3^+CD8^+$ Cytotoxic T cells and gamma delta T cells in HFD mice at 12 months age (n=9-11). Data is presented as mean ± SEM, L2=L2-IL-1β

Supplementary Figure 6.

(A) FACS analysis shows no significant increases in macrophages, $CD3^+CD4^+$ T helper cells, $CD3^+CD8^+$ Cytotoxic T cells and gamma delta T cells in L2/IL-8Tg mice at 9 months and 12 months age (n=5-8). (B) Immunohistochemistry (IHC) staining of immature myeloid cells (Ly6C) and macrophages (F4/80) in L2/IL-8Tg mice at 9 months and 12 months age (n=3) compared to L2-Chow mice from Fig 4B in 10 low power fields. (C) Representative images of goblet cells being analyzed in HE scoring. Data is presented as mean ± SEM

Supplementary Figure 7.

(A) Unifrac showing β-diversity after 16S rRNA gene sequencing of the gastro-esophageal junction of wildtype and L2-IL-1β mice treated with MNU and bile acid after removal of lactobacilli (wildtype n=4, red, L2-IL-1β n=6, blue). (B) Relative abundance of phyla after 16S rRNA gene sequencing of feces of wildtype and L2-IL-1β mice on either Control diet (n=6 each) and or HFD (n=10 each).(C) Heatmap of relative abundance of 300 most abundant OTUs of the fecal from microbiome of wildtype and L2-IL-1β

mice on Chow (n=10), Control diet (n=6) and HFD (n=10). (D) Heatmap of KEGG pathways between bacteria inhabiting wildtype and L2-IL-1β mice on Chow (n=10 each), Control diet (n=6 each) and HFD (n=10 each). Genes for KEGG analysis were estimated after 16s rRNA sequencing and predicting the microbiomes function with PICRUSt. (E) TLR2 quantitative real time PCR of L2-IL-1β mice at the age of 12 months using GAPDH as a reference (n=6 per group). Data are represented as mean ± SEM. *: $p<0.05$

Supplementary Figure 8

Diet composition of Chow, Control diet, HFD and RMH3000. (B) Body weight of L2-IL-1β mice at the age of 6 months on Chow (n=6), control diet (n=5) and HFD (n=6), mean ± SEM. (C) Macroscopic tumor score of L2-IL-1β mice at the age of 6 months on Chow (n=10), control diet (n=6) and HFD (n=12), mean ± SD. (D) Representative macroscopic image of the stomach of 6 months old L2-IL-1β mice on control diet. (E) Representative H&E staining of the stomach of 6 months old L2-IL-1β mice on control diet. (F) Representative H&E stainings of the stomach of 9 month old mice on control diet, HFD and HFD bedding transfer mice.

Supplementary Figure 9

A Model of Esophageal carcinogenesis: In the model of HFD treated L2-IL-1β mice, HFD alters the intestinal microbiome and subsequently induces distinct inflammatory cytokine responses marked by secretion of IL-8/KC and G-CSF which lead to recruitment of neutrophils and expansion of stem cells with crypt fission at the SCJ and esophagus. This ultimately accelerates the dysplasia phenotype and could be transmitted through a pathogenic microbiome or be attenuated in germfree conditions. Analysis was mainly performed and mouse SCJ and the anatomic differences between mice and humans regarding cellular and molecular changes at the SCJ need to be acknowledged.

Supplementary Methods

Cytokine array

Mouse Cytokine Array, Panel A (R&D Systems,# ARY028)) was performed according to the manufacturer's instructions and scanned for analysis. Background was subtracted by using a rolling ball algorithm (width = 50 pixels). The pixel density of each spot was then measured normalized to the reference spots and then averaged and for comparisons. For multiple comparisons the intensities were normalized to their reference spots, differences larger than 1.3 and above the background where plotted.

ELISAs

Levels of IL-8 in the tissue conditioned media and sera were assessed using MesoScale Diagnostics ELISAs as per product protocol. Cytokine levels (pg/ml) were normalized to total protein content in biopsy tissues and were expressed as pg/ul Plates were read using the MesoScale Diagnostics SECTOR imager 2400.

Immunohistochemistry

Standard immunohistochemical procedures with citrate buffer antigen retrieval (H-3300, Vector labs) were performed using the following antibodies: rabbit-anti-mouse Ki67 (Abcam, 1:500, 2h room temperature), rabbit-anti-a-SMA (Abcam, 1:400, 2 h room temperature), rabbit-antimouse DCLK (1:500, 4℃overnight) and rabbit-anti-Cxcr2 (Abcam, 1:250, 4℃ overnight). Immune cells immunohistochemistry was performed using 0.3% Triton/PBS for antigen retrieval and the following antibodies: Ratanti-F4/80 (eBioscience 1:75, 4℃ ov ernight), Rat-anti-Ly6G (eBioscience 1:100 4℃ overnight), and Rat-anti Ly6C (eBioscience 1:100, 4℃overnight). Quantification was accessed as percentage of positive cells in BE regions, which were defined as the region between squamous epithelium and oxyntic mucosa of the stomach or as number of positive cells in the esophagus/squamous epithelium in 10 low power fields of vision.

Transcriptional profile analysis

Total RNA from SCJ and forestomach tissues were extracted by TRIzol reagent (Invitrogen) according to the manufacturers protocol. Expression profiling was accomplished using Mouse gene 2.1 Affymetrix arrays. Differential expression in relation to WT mouse control groups was determined using Limma[1] as implemented in oneChannelGUI[2] operating as part of the Bioconductor Suite[3] in the R statistical computing environment[4]. A significance cutoff of the Benjamini-Hochberg False Discovery Rate <0.05 was used[5]. Estimates of the statistical significance of overlap between gene

sets were performed using the chi-square test[8] as implemented in R. Raw data have been deposited in National Center for Biotechnology Information's Gene Expression Omnibus (GEO) (GSE103616). Functional annotation of phenotypes was performed by gene set enrichment analysis (GSEA) using the MSigDB database v5.2 where each phenotype was represented by three mice. An internal IL8 dependent gene set was generated comparing L2-IL1B/IL8 with control p2-IL1β mice using differentially expressed genes that had log2 fold change of +/- 0.6, equivalent to an increase by a factor of at least 1.5 (equivalent to a 50% increase) in L2-IL1B/IL8Tg mice. Additional gene sets reflecting a mouse specific epithelial (cancer) stem cell phenotype (STEM-CELL-GENE-SET[6], GENES-IN-MOUSE-ADULT-TISSUE-STEM-MODULE[7]) were also applied.

3-D organoid culture

The SCJ tissue of mice was processed for organoid culture as previously described[8]. Organoids were cultured for 7-14 days prior to the co-culture with lean patient serum or obese patient serum or sera from mice fed chow or HFD for 24, 48 and 72h. For neutrophil co-culture experiments, neutrophils were isolated daily from spleens of 9-12-month-old L2-IL1B mice by using anti-Ly6G MACS magnetic microbeads system according to the manufacturer's protocol (MiltenyiBiotec). Then neutrophils were added to each well at Day-1 and Day-2, and neutrophils then were allowed to infiltrate organoids for up to 120h.

Microbiome analysis

For human microbiota analysis, Cytosponge samples were analyzed from patients with non-dysplastic and dysplastic BE and control patients with dyspepsia from a cohort that was published previously[9]. Microbial DNA extraction and 16S rRNA gene amplicon sequencing was performed as previously described and analysed by using mothur [10]. Data have been deposited in the European Nucleotide Archive under accession number ERP005191. For mouse microbiome, fecal samples were taken during the necropsy of the experimental mice. DNA purification and 16s sequencing was performed by the Tataa Biocenter in Gothenburg using MiSeq sequencers. The analysis of the sequences was performed using QIIME [11].

Real-Time PCR Analysis

Superscript II Reverse Transcriptase (Invitrogen) was used for synthesis of cDNA. Real-time PCR analysis with a Power SYBR Green PCR Master Mix (Applied Biosystems) was performed on a

LightCycler 480 Instrument (Roche). RNA levels were normalized to GAPDH and calculated as copies per 10000 copies of GAPDH . Primer sequences are listed in Supp. Table 1.

Patient Serum profile:

Serum was collected from lean (men; n=10, women; n=9) and obese (men; n=10, women; n=10) volunteers at Rockefeller University (New York, NY). The median age of the male and female cohorts were 48 years (range 40-68) and 56 years (45-66) respectively. The median BMI of the lean and obese men was 22.4 (range 19.5-25) and 37.75 (range 35.2- 49.7), respectively, while the median BMI of the lean and obese women was 22.4 (range 19.7- 24.9) and 38.1 (range 36.1-46.1), respectively. Serum was stored at -80℃ and then hormone and cyto kine levels in serum were measured by ELISA

Flow cytometry

Single-cell suspensions were generated as previously described[1]. The following antibodies were used: APC-anti-F4/80, APC-e780-anti-cd11b1β, Alexo700-anti-Ly6G, eFluor450-lanti- CD45, PE-Ly6C, eFluor450-anti-CD4, APC-CD8a, FITC- anti-CD3, APCe780-NK1.1, PE-antigamma delta TCR. 7-AAD was used to quantify live cells. (All antibodies were purchased from eBioscience). FACS data were acquired on a Gallios flow cytometer (Beckman Coulter) and analyzed using FlowJo software (TreeStar).

Reference

1. Smyth GK. Linear Models and Empirical Bayes Methods for Assessing Differential Expression in Microarray Experiments. Statistical Applications in Genetics and Molecular Biology 2004;3:Article 3, http://www.bepress.com/sagmb/vol3/iss1/art3/.
2. Sanges R, Cordero F, Calogero RA. oneChannelGUI: a graphical interface to Bioconductor tools, designed for life scientists who are not familiar with R language. Bioinformatics 2007;23:3406-8.
3. Gentleman RC, Carey VJ, Bates DM, et al. Bioconductor: open software development for computational biology and bioinformatics. Genome Biol 2004;5:R80.
4. Ihaka R, Gentleman R. R: A language for data analysis and graphics. Journal of Computational and Graphical Statistics 1996;5:299-314.
5. Benjamini Y, Hochberg Y. Controlling the false discovery rate; A practical and powerful approach to multiple testing. J. Roy. Stat. Soc. Ser. B 1995;57:289-300.
6. van der Flier LG, van Gijn ME, Hatzis P, et al. Transcription factor achaete scute-like 2 controls intestinal stem cell fate. Cell 2009;136:903-12.
7. Wong DJ, Liu H, Ridky TW, et al. Module map of stem cell genes guides creation of epithelial cancer stem cells. Cell Stem Cell 2008;2:333-44.
8. Pastula A, Middelhoff M, Brandtner A, et al. Three-Dimensional Gastrointestinal Organoid Culture in Combination with Nerves or Fibroblasts: A Method to Characterize the Gastrointestinal Stem Cell Niche. Stem Cells Int 2016;2016:3710836.
9. Elliott DR, Walker AW, O'Donovan M, et al. A non-endoscopic device to sample the oesophageal microbiota: a case-control study. Lancet Gastroenterol Hepatol 2017;2:32-42.
10. Schloss PD, Westcott SL, Ryabin T, et al. Introducing mothur: open-source, platform-independent, community-supported software for describing and comparing microbial communities. Appl Environ Microbiol 2009;75:7537-41.
11. Caporaso JG, Kuczynski J, Stombaugh J, et al. QIIME allows analysis of high-throughput community sequencing data. Nat Methods 2010;7:335-6.

Supplementary Figure 1:

A

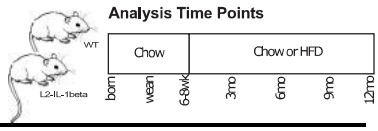

	V1124-000	S5745-E712
Dietary components	**Standard Chow**	**HFD Palm oil**
Gross Energy (GE)	16.7 MJ/kg	21.9 MJ/kg
Metabolizable Energy (ME)	14.0 MJ/kg	19.7 MJ/kg
Protein [kJ%]	27	18
Fat [kJ%]	12	48
Carbohydrates [kJ%]	61	34
Crude Nutrients [%]		
Protein	22.0	21.2
Fat	4.5	25.1
Fiber	3.9	5.0
Ash	6.2	5.3
Starch	34.2	26.7
Sugar	5.1	6.1
N free extracts	51.2	37.7
Amino Acids [%]		
Lysine	1.5	1.8
Methionine	0.5	0.8
Met + Cys	0.4	1.1
Threonine	0.9	0.9
Tryptophan	0.3	0.3
Minerals [%]		
Calcium	1.0	0.9
Phosphorus	0.7	0.7
Sodium	0.2	0.2
Magnesium	0.2	0.2
Vitamins [IU/kg]		
Vitamin A	25,000.00	18,000.00
Vitamin D_3	1,500.00	1,800.00
Vitamin E	135	180
Fatty acids [%]		
C 12:0	-	0.01
C 14:0	0.01	0.21
C 16:0	0.54	9.18
C 18:0	0.14	1.11
C 20:0	0.02	0.1
C 16:1	0.02	0.05
C 18:1	1.03	9.19
C 18:2	2.42	4.67
C 18:3	0.28	0.35

B

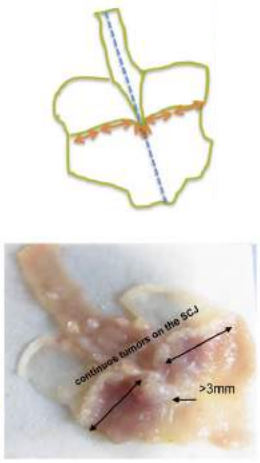

C

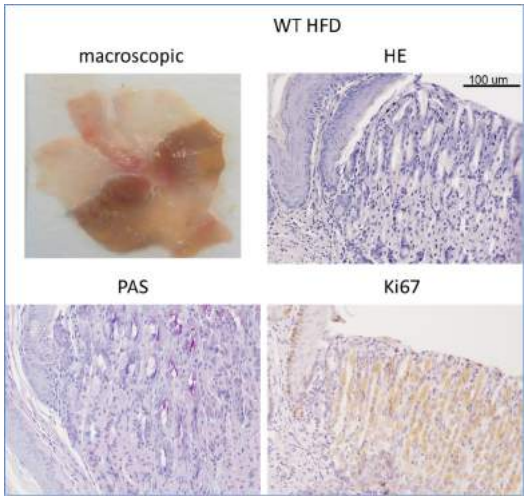

D

Tumor size		Tumor coverage	
0	No abnormalities	0	No abnormalities
1	<0.5 mm	1	Focal tumors (<20%)
2	>0.5-1 mm	2	Partial tumors (20-50%)
3	>1-2 mm	3	Increased tumors (>50-80%)
4	>2-3 mm	4	Continuous tumors (>80%)

E

Score	Inflammation	Metaplasia	Dysplasia
0	no inflammation no immune cell influx	no metaplasia	no dysplasia
1	mild inflammation up to 10 immune cells	rare mucus cells	superficial epithelial atypia
2	moderate inflammation up to 30 immune cells	single metaplastic glands	atypia in glandular complexity
3	severe inflammation more than 30 immune cells	multiple metaplastic glands	low grade dysplasia
4			high grade dysplasia

F

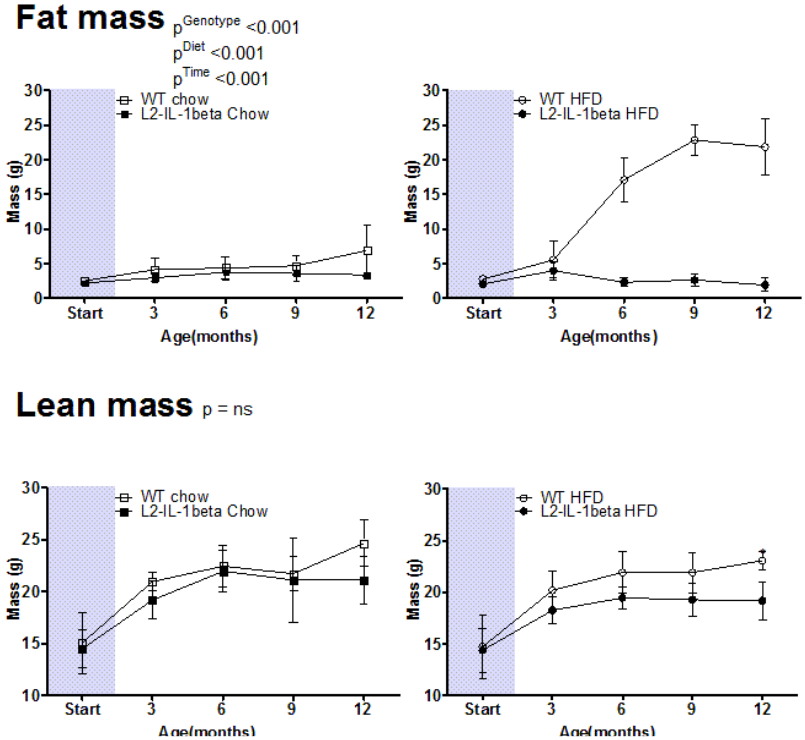

Supplementary Figure 2:

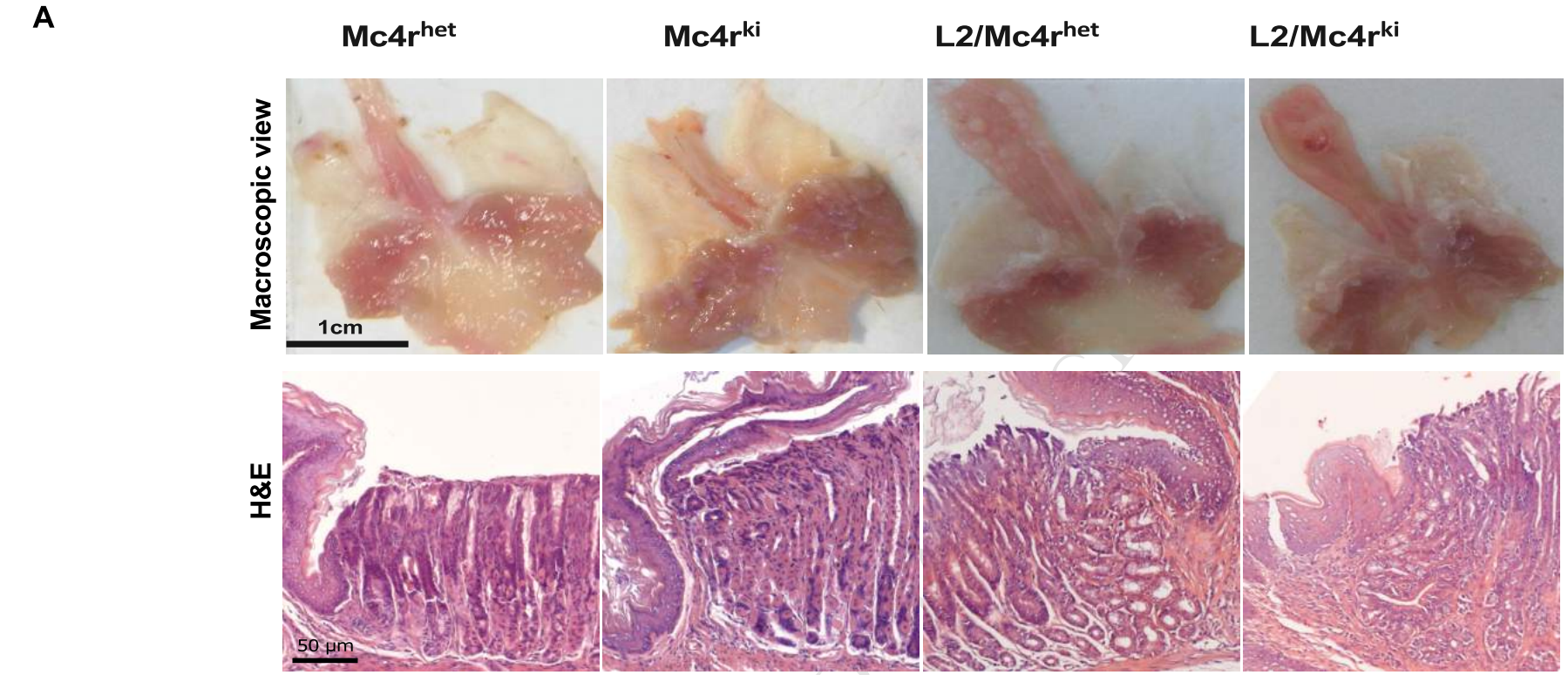

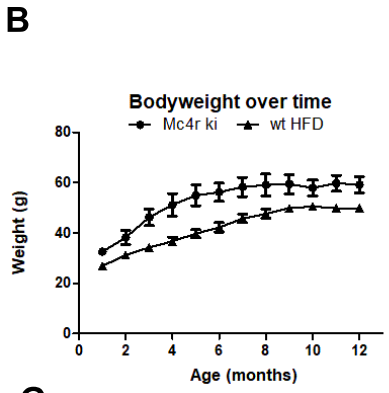

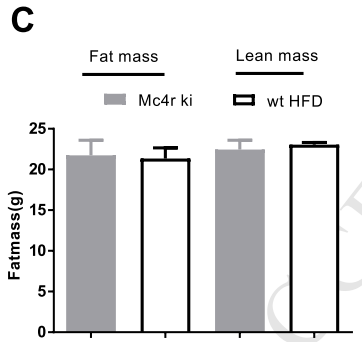

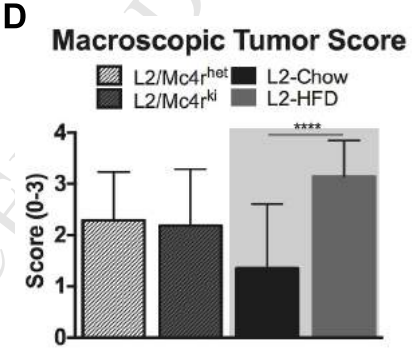

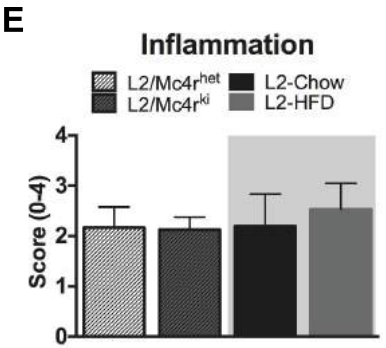

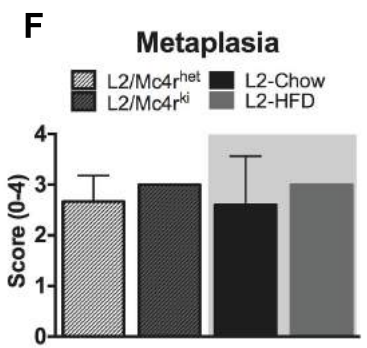

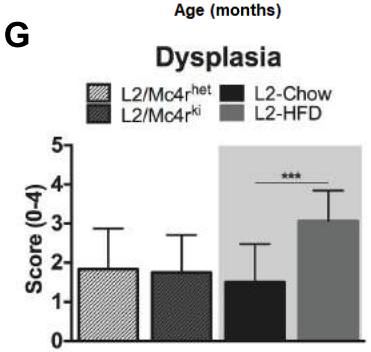

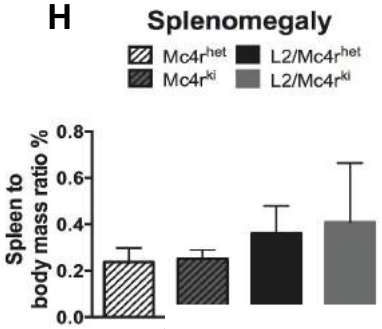

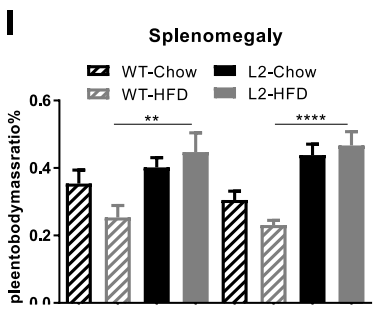

Supplementary Figure 3:

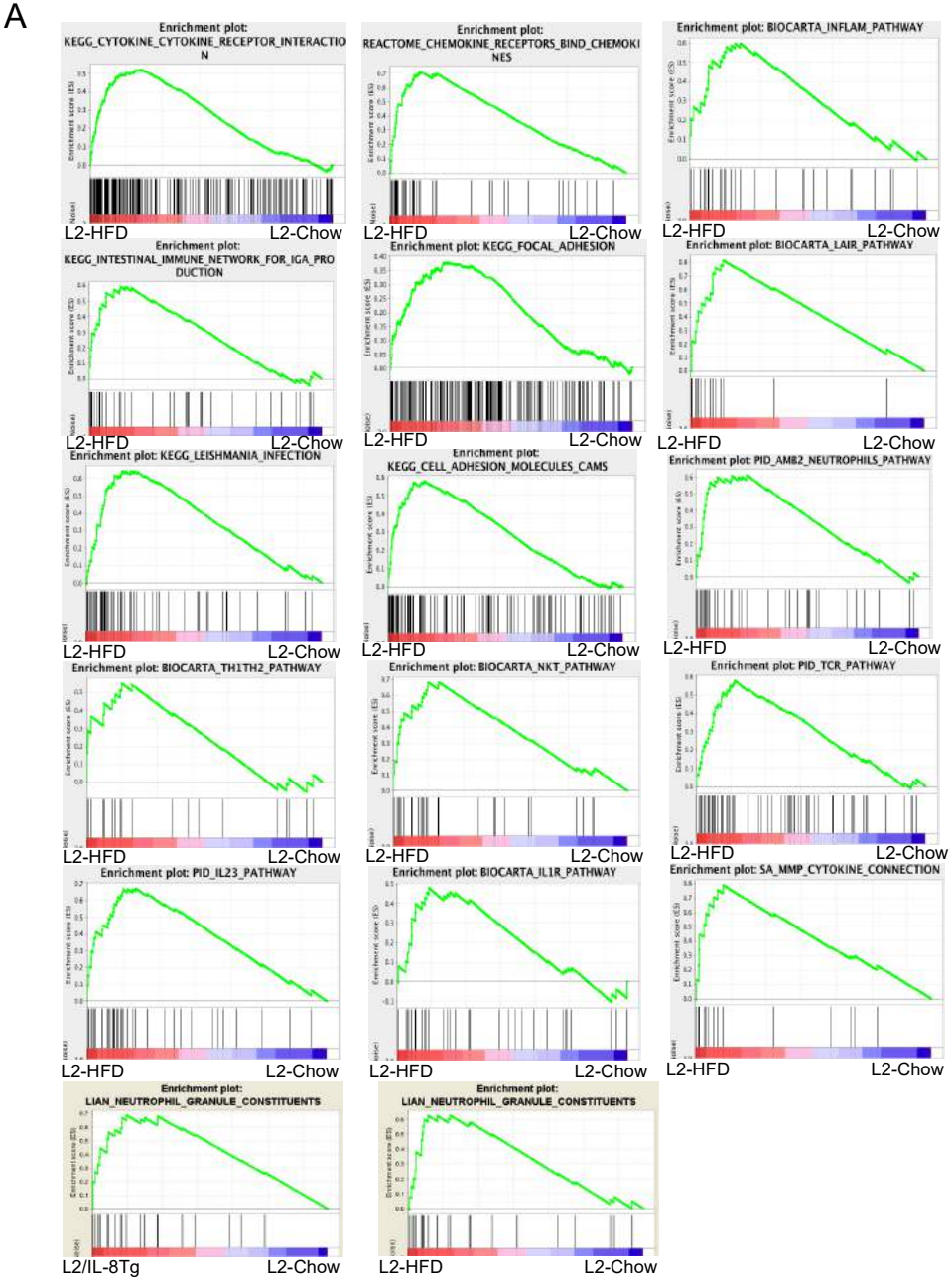

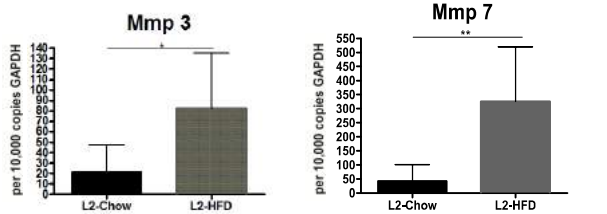

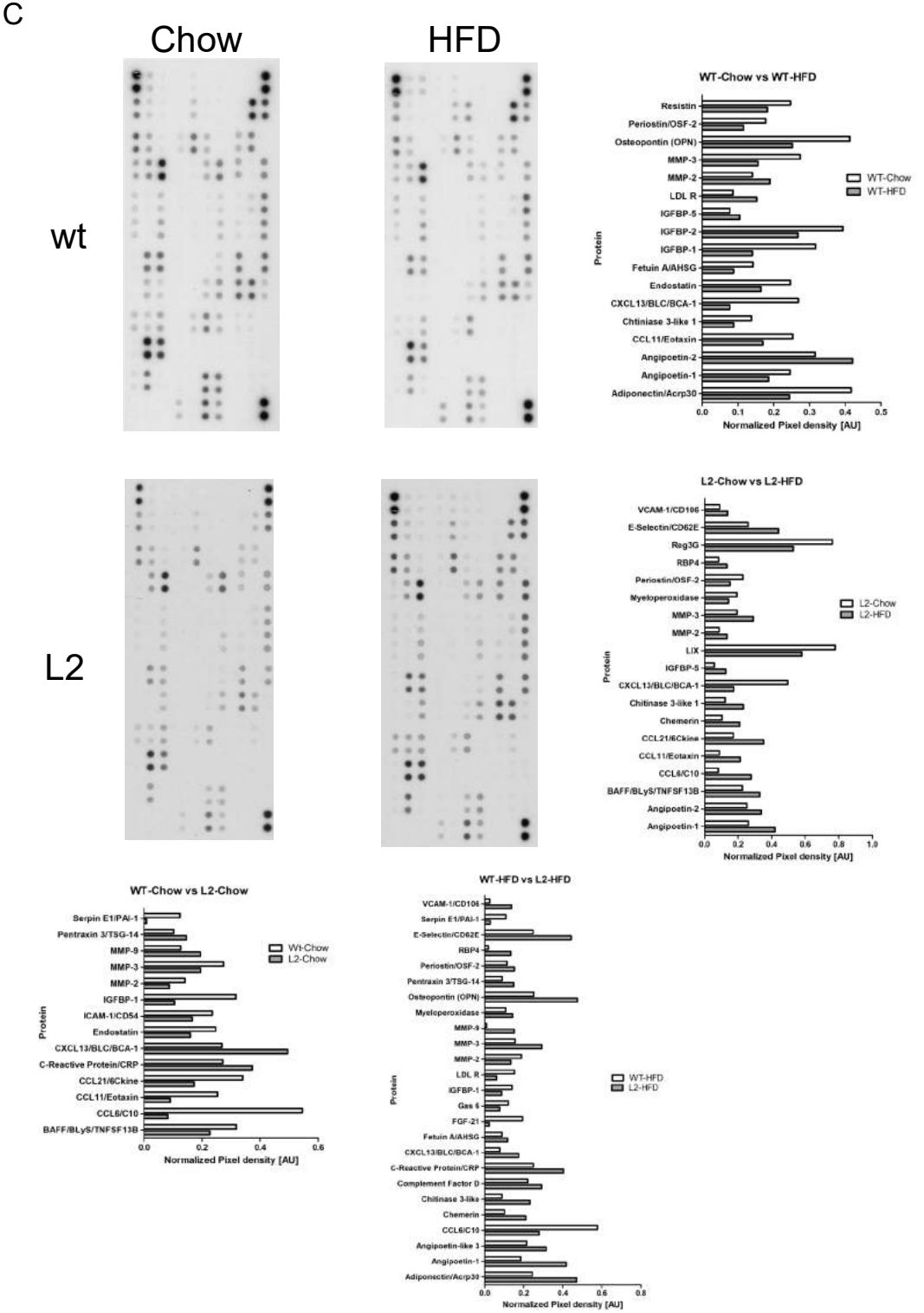

Supplemental Figure4 :

A

Serum profiles of lean and obese patients

Variables	All	Normal	Obese	p.value
BMI				
Males	30.1 (19.5, 49.7)	22.4 (19.5,25)	37.75 (35.2, 49.7)	<0.001
Females	36.1 (19.7, 46.1)	22.4 (19.7,24.9)	38.1 (36.1,46.1)	<0.001
Age				
Males	48 (40, 68)	48.5 (40,66)	48 (42,68)	1
Females	56 (45, 66)	57 (47,61)	56 (45,66)	0.682
CRP				
Males	1.21 (0.25, 12.42)	0.53 (0.25,4.04)	2.78 (0.52,12.42)	0.015
Females	2.74 (0.12, 15.04)	0.28 (0.12,3.6)	6.14 (1.71,15.04)	<0.001
Adiponectin				
Males	5.48 (2.61, 22.75)	6.59 (4.34,14.68)	5.04 (2.61,22.75)	0.218
Females	10.37 (2.55, 26.36)	18.04 (10.26,26.36)	6.17 (2.55,19.24)	<0.001
Leptin				
Males	6.53 (0.14, 74.41)	1.04 (0.14,3.58)	19.51 (9.47,74.41)	<0.001
Females	32.33 (2.77, 68.98)	9.28 (2.77,37.75)	47.87 (20.76,68.98)	<0.001
LeptAdipRatio				
Males	0.44 (0.02, 13.95)	0.14 (0.02,0.46)	4.87 (0.42,13.95)	<0.001
Females	2.83 (0.12, 21.3)	0.54 (0.12,2.83)	8.59 (1.08,21.3)	<0.001
Insulin				
Males	5.15 (1.7, 51.39)	3.78 (1.7,6.81)	12.47 (5.03,51.39)	<0.001
Females	7.92 (3.45, 28.1)	4.79 (3.45,9.3)	11.58 (6.85,28.1)	0.001
Glucose				
Males	84.06 (69.34, 109.01)	78.95 (69.34,98.79)	89.77 (73.54,109.01)	0.028
Females	89.77 (74.14, 111.41)	84.36 (74.14,93.38)	102.39 (80.16,111.41)	0.003
IL-6				
Males	2.1 (0.68, 6.69)	1.72 (0.68,4.95)	2.65 (1.4,6.69)	0.052
Females	2.41 (0.81, 4.57)	1.26 (0.81,1.96)	3.14 (2.41,4.57)	<0.001
Testosterone				
Males	7.19 (4.8, 13.6)	8.2 (5.54,10.02)	5.94 (4.8,13.6)	0.052
Estradiol				
Females	20.58 (5.92, 67.31)	14.51 (5.92,67.31)	26.52 (17.24,34.16)	0.006
SHBG				
Females	55.5 (8.25, 242.97)	86.03 (38,242.97)	36.89 (8.25,76.29)	<0.001
Estradiol:SHBGRatio				
Females	0.28 (0.08, 2.5)	0.15 (0.08,0.28)	0.78 (0.23,2.5)	<0.001

B

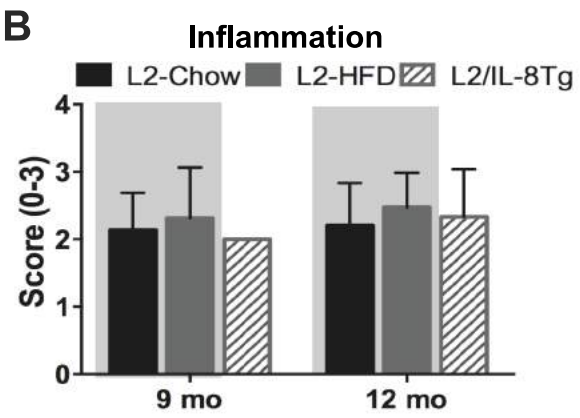

C

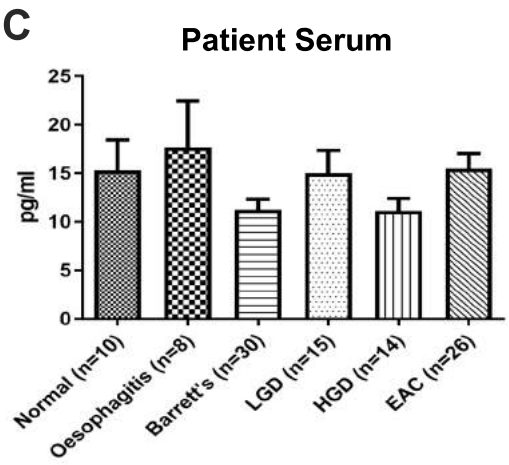

D

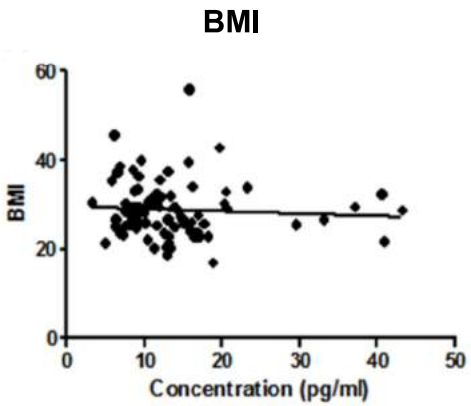

E

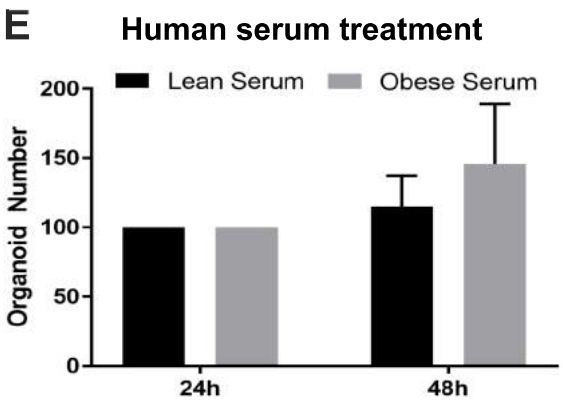

Supplemental Figure5 :

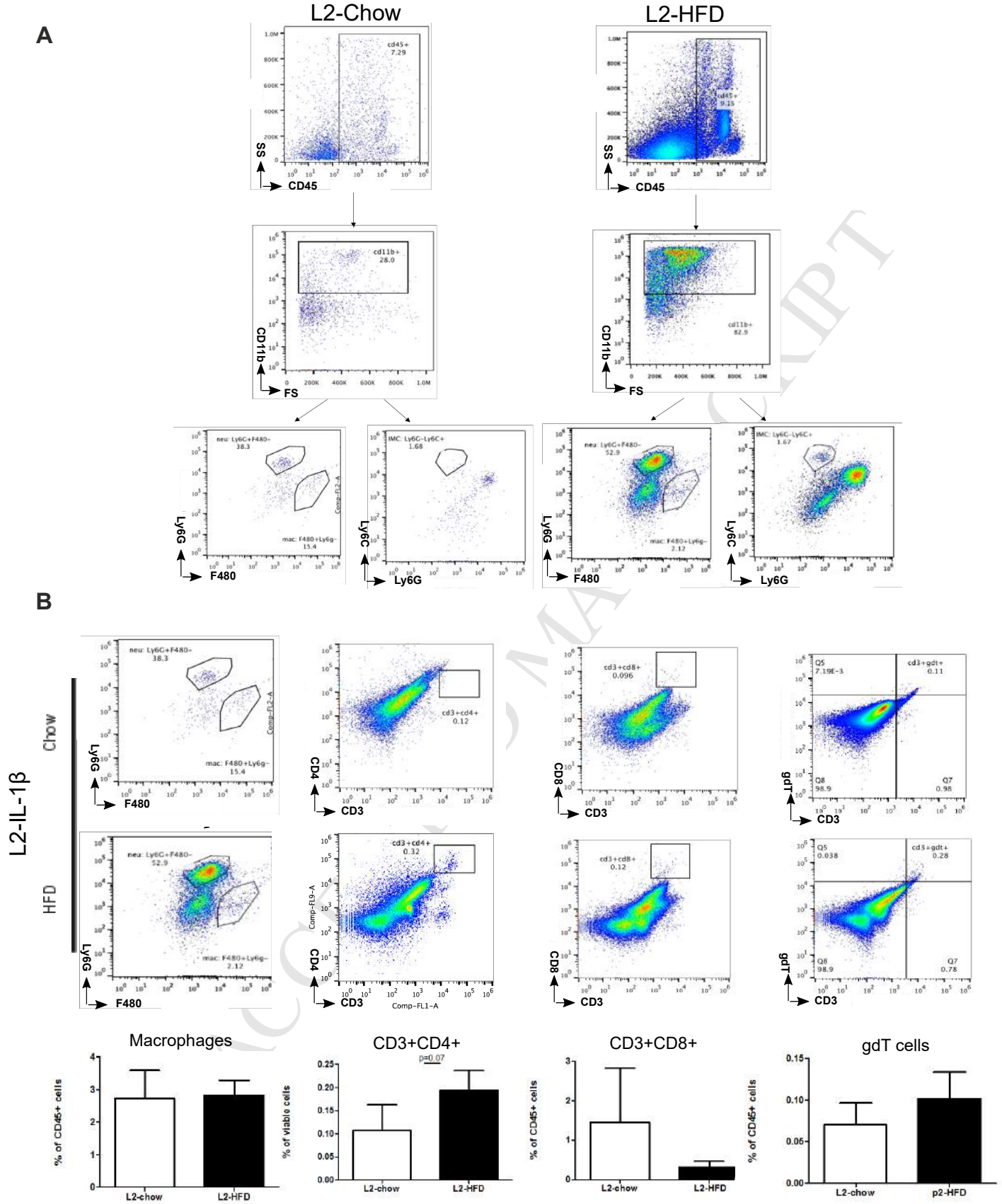

Supplemental Figure6

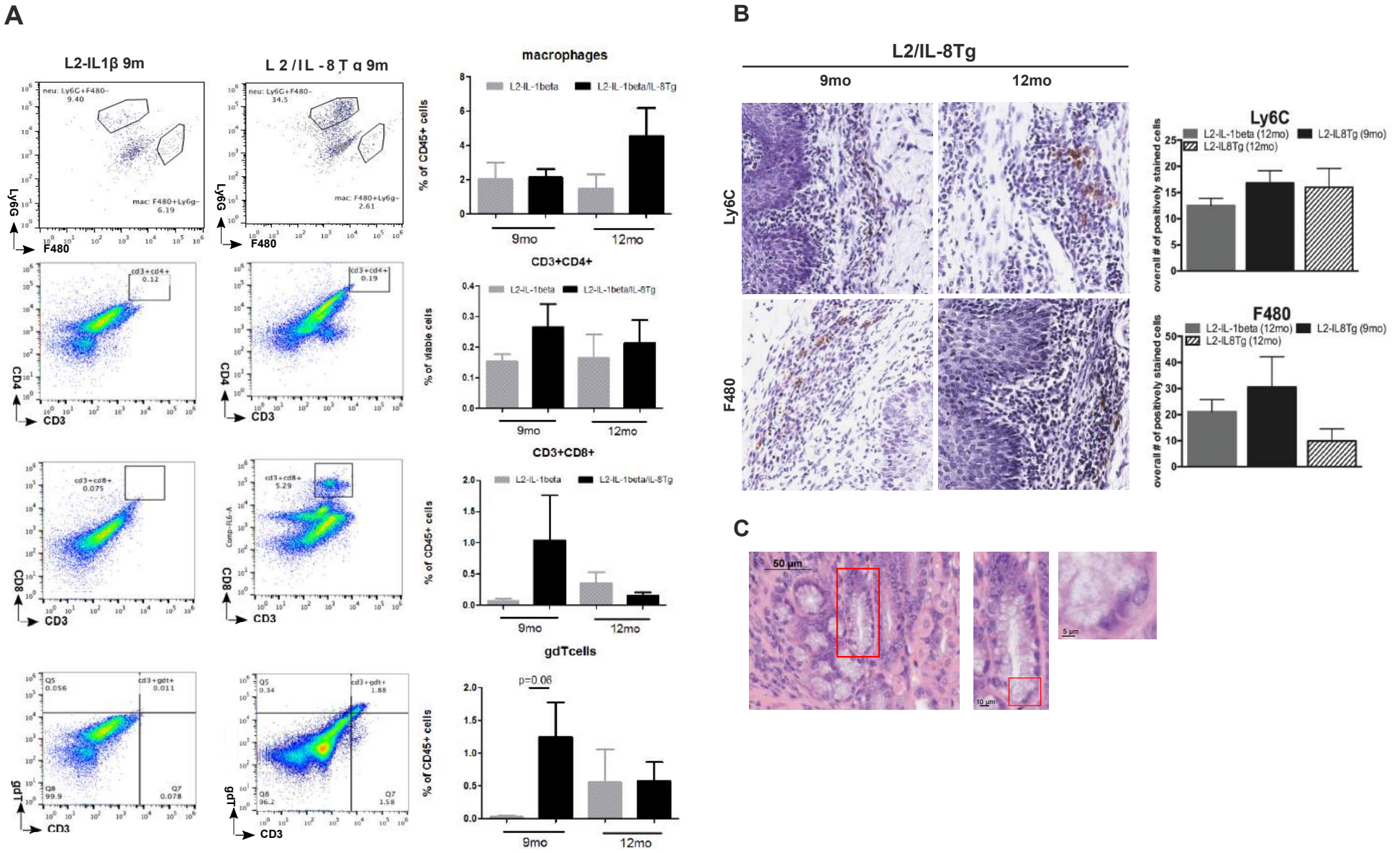

Supplemental Figure 7

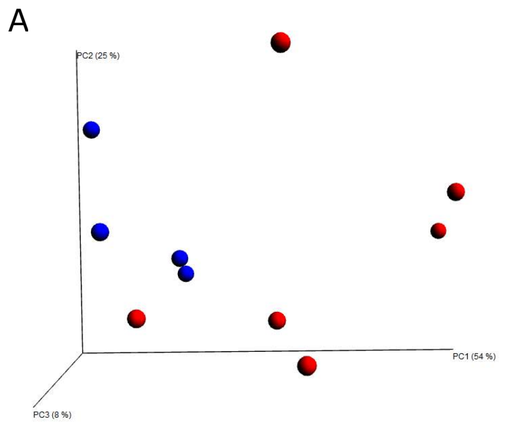

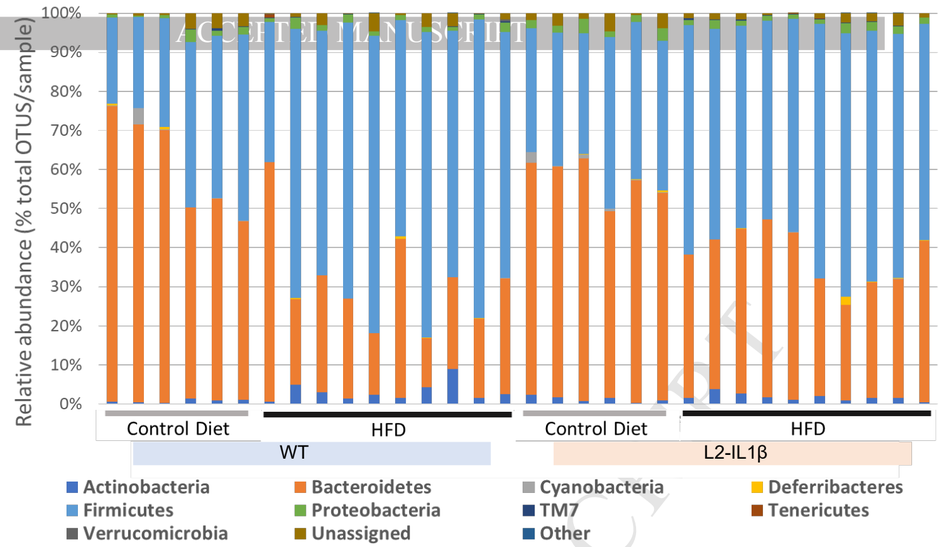

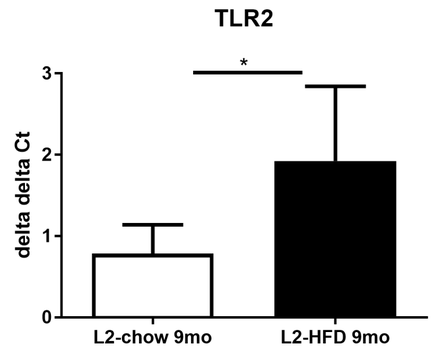

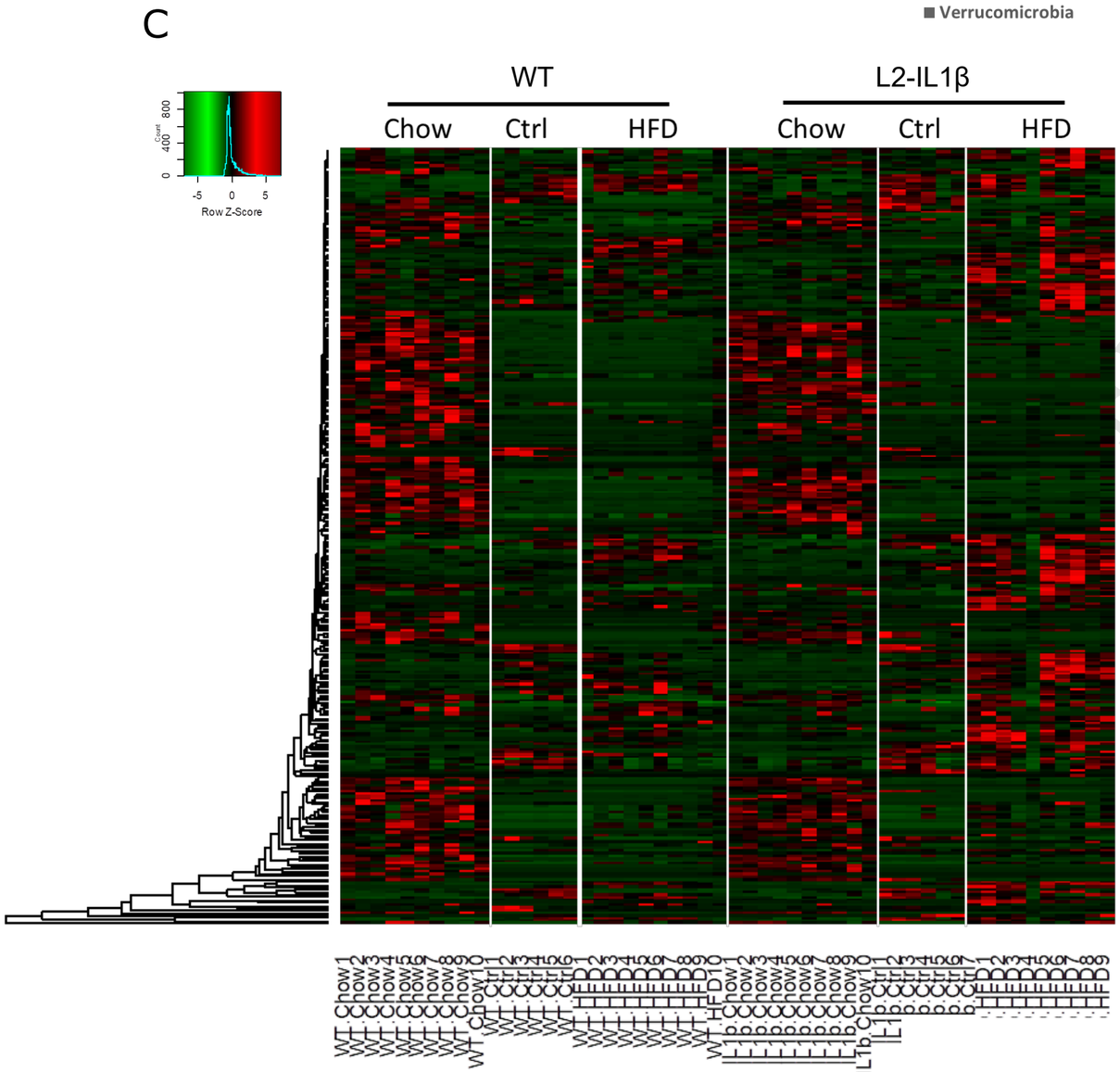

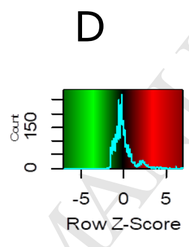

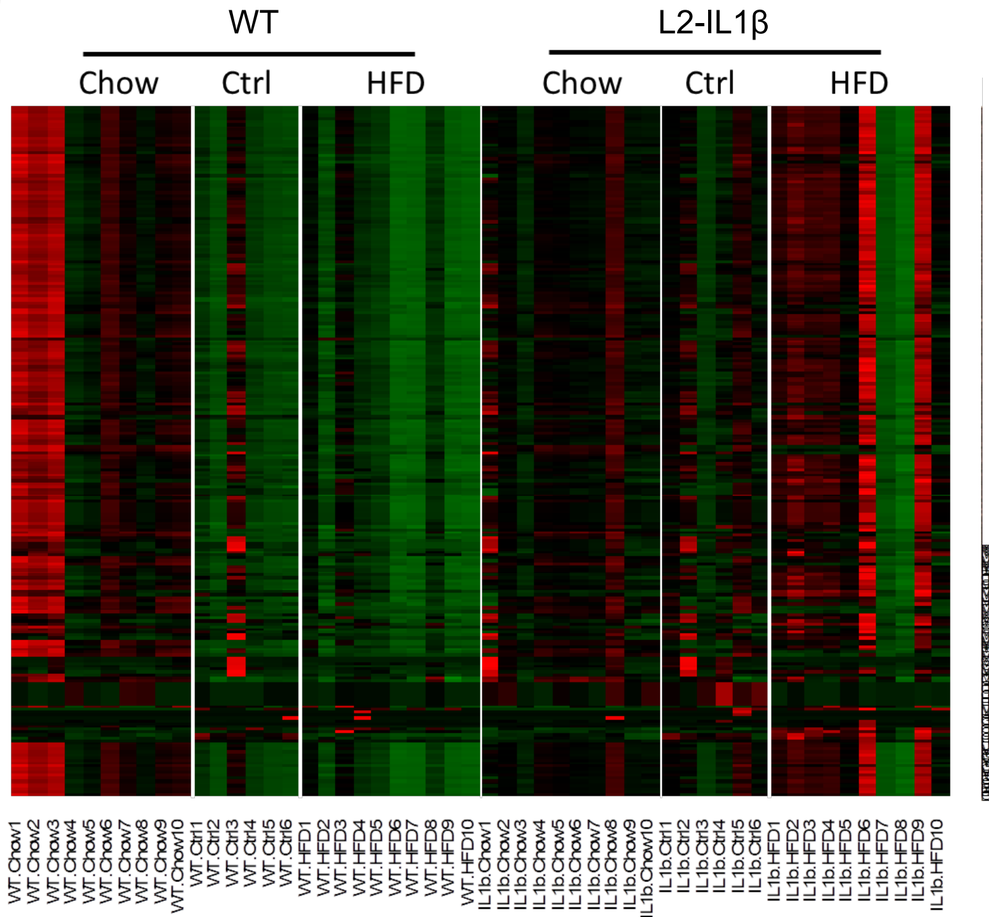

Supplemental Figure8

A

Dietary components	V1124-000 Standard Chow	S5745-E712 HFD Palm oil	S5745-E702 Control	RMH3000 Germfree Chow
Gross Energy (GE)	16.7 MJ/kg	21.9 MJ/kg	16.9 MJ/kg	17.2
Metabolizable Energy (ME)	14.0 MJ/kg	19.7 MJ/kg	15.3 MJ/kg	13.3888
Protein [kJ%]	27	18	23	23
Fat [kJ%]	12	48	13	14
Carbohydrates [kJ%]	61	34	64	60
Crude Nutrients [%]				
Protein	22.0	21.2	21.2	22.5
Fat	4.5	25.1	5.1	5.4
Fiber	3.9	5.0	5.0	4.0
Ash	6.2	5.3	5.3	6.1
Starch	34.2	26.7	45.9	30.4
Sugar	5.1	6.1	6.1	1.3
N free extracts	51.2	37.7	56.8	52.0
Amino Acids [%]				
Lysine	1.5	1.8	1.8	1.3
Methionine	0.5	0.8	0.8	0.5
Met + Cys	0.4	1.1	1.1	0.8
Threonine	0.9	0.9	0.9	0.8
Tryptophan	0.3	0.3	0.3	0.3
Minerals [%]				
Calcium	1.0	0.9	0.9	1.0
Phosphorus	0.7	0.7	0.7	0.8
Sodium	0.2	0.2	0.2	0.3
Magnesium	0.2	0.2	0.2	0.2
Vitamins [IU/kg]				
Vitamin A	25,000.00	18,000.00	18,000.00	29,000.00
Vitamin D_3	1,500.00	1,800.00	1,800.00	2,400.00
Vitamin E	135	180	180	75
Fatty acids [%]				
C 12:0	-	0.01	0.01	NA
C 14:0	0.01	0.21	0.02	NA
C 16:0	0.54	9.18	0.58	NA
C 18:0	0.14	1.11	0.18	NA
C 20:0	0.02	0.1	0.02	NA
C 16:1	0.02	0.05	0.01	NA
C 18:1	1.03	9.19	1.29	NA
C 18:2	2.42	4.67	2.65	1.73
C 18:3	0.28	0.35	0.29	0.16

B

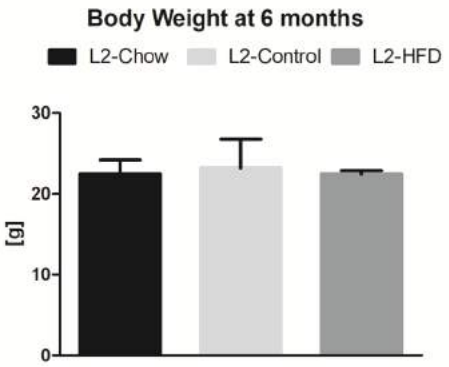

D

C

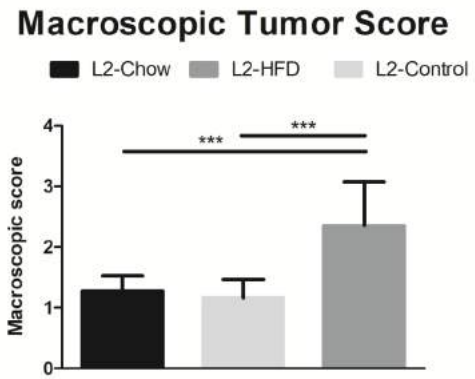

E

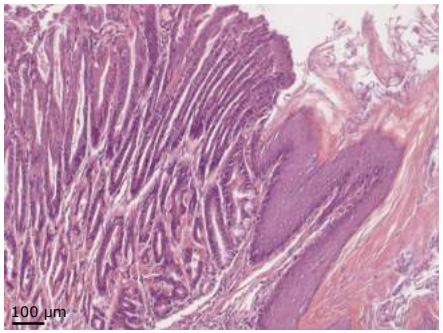

F

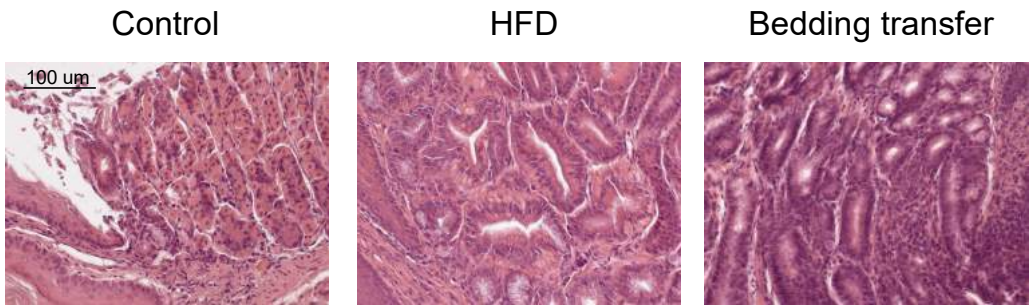

Supplementary Figure9: